Influence of glacial influx on the hydrodynamics of Admiralty Bay, Antarctica - a case study based on combined hydrographic measurements and numerical modeling

M. Osińska[1], and A. Herman[2]

[1]University of Gdańsk, Faculty of Oceanography and Geography, Gdańsk Poland

[2]Institute of Oceanology, Polish Academy of Sciences, Sopot, Poland.

Corresponding author: Maria Osińska maria.osinska@phdstud.ug.edu.pl

Key Points:

- Investigation of the distinct traits of Antarctic glacial bay hydrodynamics based on vast hydrographic measurements and modeling results
- Assessment of the influence of glacial discharges on water levels, circulation patterns and freshwater content
- Estimation of seasonal variations in glacial influx volumes over a four-year period with the highest temporal resolution to date

Abstract

This study investigates the impact of glacial water discharges on the hydrodynamics of Admiralty Bay (AB) in the South Shetland Islands, a wide bay adjacent to twenty marine-terminating glaciers. From December 2018 until February 2023, AB water properties were measured on 136 days. This dataset showed that a maximally two-layered stratification occurs in AB and that glacial water is always the most buoyant water mass. Using the Delft3D Flow, a three-dimensional hydrodynamical model of AB was developed. During tests, the vertical position and initial velocity of glacial discharges have been shown to be insignificant for the overall bay circulation. Fourteen model scenarios have been calculated with an increasing glacial influx added. The AB general circulation pattern consists of two cyclonic cells. Even in scenarios with significant glacial input, water level shifts and circulation are predominantly controlled by the ocean. Glacial freshwater is carried out of AB along its eastern boundary in a surface layer no thicker than 60 m. Within the inner AB inlets, significant glacial influx produces buoyancy-driven vertical circulation. Using an innovative approach combining hydrographic and modeling data, a four-year, unprecedentedly high-resolution timeseries of glacial influx volumes into AB has been produced. On average, glacial influx summer values are >10 times greater than in spring and winter and 3 times higher than in autumn. The annual glacial influx into AB was estimated at 0.525 Gt. Overall, it was demonstrated how the topography and forcing controlling the hydrodynamics of an Antarctic bay differs from that of well-studied northern-hemisphere fjords.

Plain Language Summary

The purpose of this research was to investigate how water from glaciers impacts the flow of water in Admiralty Bay (AB) in Antarctica. Multiple measurements of the parameters of AB water were taken, and a 3D hydrodynamical model was built. Fourteen model scenarios with varying amounts of glacier water were calculated. AB water typically flows in two clockwise cells. Even when large amounts of glacial water are supplied to AB, the ocean controls changes in water level and the overall flow pattern. A thin surface layer of freshwater from glaciers flows out of AB on its eastern side. A large amount of glacial water might create alterations in flow patterns in the inner AB regions. By comparing measurement and model data, a four-year time series of glacial influx volumes into AB was created. The glacial water inflow is more than ten times greater in the summer than in the spring and winter, and three times greater in the autumn. It is anticipated that 0.525 gigatons of glacial water are released into AB each year. Overall, it was demonstrated how the Antarctic glacial bay differs from northern hemisphere fjords.

1 Introduction

Antarctic coastal areas play a crucial role within the broader Southern Ocean system. In the West Antarctic Peninsula (WAP) region more than 650 marine terminating glaciers are draining into the ocean, mostly through glacial bays (Cook et al., 2016). Glaciers are significant contributors to global sea level rise due to their high accumulation and ablation rates (Gregory et al., 2013). The glacial water inflow to the ocean influences a wide range of climate-sensitive processes, including shifts in the carbon cycle, ocean acidification, and reorganization of water column stratification (IPCC, 2022). With it, additional carbon, iron, and manganese are transported into the ocean, stimulating phytoplankton blooms and impacting local food chains (Forsch et al., 2021; Schloss et al., 2012). In order to comprehend the impact of glacial water on

the Southern Ocean, it is imperative to understand the hydrodynamics of glacial bays. In particular, it is crucial to understand how the bay dynamics responds to variations in the volume of glacial water influx in an era of unavoidable acceleration of the West Antarctic ice sheet melt rates (Naughten et al., 2023). This is because it is expected that unprecedentedly large amounts of freshwater will be introduced into Antarctic coastal waters in the near future, which could have complex and unanticipated consequences for regional hydrodynamics.

Freshwater from glaciers, both from subglacial discharges and submarine melting, mixes with ambient water, forming Glacially Modified Water (GMW; Straneo & Cenedese, 2015). To date, the majority of studies into GMW transport and its influence on coastal hydrodynamics have concentrated on fjords in the northern hemisphere, which differ geomorphologically from Antarctic glacial bays (Cottier, et al., 2010). Fjords in Greenland, Alaska, and Spitsbergen are typically long, narrow, and deep. In these basins, described by a large Rossby internal radius (Cottier et al., 2010; Valle-Levinson, 2022), the role of cross-fjord circulation is often minimal, allowing for simplified analysis and modeling in only two dimensions (Mortensen et al., 2013; Motyka et al., 2003; Sciascia et al., 2013).

Motyka et al. (2003) demonstrated that circulation in narrow fjords may be reduced to a single vertical cell with GMW flowing away from the glacial front in the surface layer and ocean waters flowing in towards the front beneath it, upwelling along the glacier, entrained by rising subglacial discharge. This basic model, however, is inadequate in larger Greenlandic fjords, since glacial waters do not always reach the surface due to a larger scale and complex water column stratification (Sciascia et al., 2013; Straneo et al., 2011).

"Unmixing GMW" methods based on hydrographic data are the most widely used techniques for quantifying and tracking pathways of glacial water in the ocean (Bartholomaus et al., 2013; Jenkins, 1999; Jenkins & Jacobs, 2008; Mortensen et al., 2013; Straneo et al., 2011). When GMW spreads in a narrow fjord from a singular glacial front, this analysis can provide almost the entire story of GMW transport since it shows the spatial variability of freshwater content as a function of depth and distance from the outlet. However, in wide bays with complex bathymetry and several marine terminating glaciers, freshwater, after its initial injection, can circulate within the bay, mixing with ambient waters and providing feedback on other ice−water fronts. Three-dimensional (3D) modeling is required to characterize such circulation, and it has been applied successfully in several studies. However, the setup used most commonly describes long, deep, and narrow fjords with a single glacial front (e.g., Cowton et al., 2015; Sciascia et al., 2013; Slater et al., 2018; Xu et al., 2012).

Our study area, Admiralty Bay (AB), is located in the South Shetland Islands, in the northern WAP region. AB has distinctive traits of Antarctic bays rarely seen in the northern hemisphere: it is wide, has a complex coastline, and is adjacent to twenty marine terminating glaciers.

Although previous studies into GMW impact have predominantly focused on the northern hemisphere, recent research has also expanded our understanding of the hydrodynamics of the glacial bays of the WAP region. In Marguerite Bay, seasonal freshwater content variations were measured, and its sources were identified (Clarke et al., 2008; Meredith et al., 2010). The waters of Marguerite Bay and Barilari Bay were shown to be subject to intrusions of warm Upper Circumpolar Deep Water (UCDW), which can be an additional driver of glacial melting (Cape et al., 2019; Clarke et al., 2008). The study by Cape et al., (2019) looked at the impact of

glacial-oceanic interactions on coastal dynamics in Barilari Bay. Specifically, the study concentrated on the formation of surface GMW plumes and its consequences for local biogeochemistry. Lundesgaard et al. (2020) conducted a thorough investigation of the physical properties of water in Andvord Bay, where the influence of UCDW was found to be limited due to the presence of a sill at the bay's outlet. Based on these findings, Hahn-Woernle et al. (2020) demonstrated the significant role of surface water thermodynamics in the bay system. Lundesgaard et al. (2019) showed how episodic strong wind events can play a substantial role in the export of GMW from Andvord Bay. Meredith et al. (2018) investigations in Potter Cove, King George Island, have revealed the characteristics of glacial meltwater spreading from land-terminating Fourcade Glacier, a glacial form that is more prevalent in the South Shetlands than in the southern WAP region. In conclusion, our knowledge of the Antarctic glacial bay systems has grown over the past few years; a number of hydrodynamical drivers, such as the presence of UCDW, wind, heat content of the upper ocean, and glacial termini type, have been studied. The seasonal variations and long-term increase in glacial runoff have been shown through the analysis of hydrographic and glaciological data (Clarke et al., 2008; Meredith & King, 2005; Vaughan, 2006). However, no research has been conducted to investigate how these changes affect Antarctic bay water level shifts, circulation patterns, and freshwater distribution. This is the goal of this study.

The structure of this paper follows the logical reasoning underlying this project, in which numerical modeling is based on the conclusions from the analysis of observational data. The study area is described in Section 2, followed by the details of *in situ* measurement methodology (Section 3.1). Section 3.2 provides a general overview of water property variations in AB. A 3D circulation model was developed based on the conclusions of Section 3.2 (technical details in Section 4.1). The problem of determining the appropriate location of glacial water injection points in the model was essential. Therefore, Section 4.2 describes its theoretical background and presents the results of model test runs conducted to examine it. The model was run in fourteen scenarios with an increasing glacial influx volume. The findings revealed the character and magnitude of glacial water's impact on water level variations, circulation, freshwater thickness (FWT), and pycnocline depth in the bay (Section 4.3). This enabled identification of boundaries between regions dominated by glacially and tidally-driven circulation patterns (Spall et al., 2017). Finally, in Section 5, an attempt was made to estimate the glacial runoff volume into AB. This estimate was based on a novel approach in which differences between modeling results and *in situ* measurements were used to select an optimal (most probable) influx volume at a given time instance, yielding a 136-record-long timeseries of glacial influx volumes in the period from December 2018 to February 2023 (Mortensen et al., 2014; Sciascia et al., 2013; Straneo, et al., 2011). The results are followed by a discussion and conclusions in Section 6.

This research provides one of the first assessments of the sensitivity of an Antarctic bay's hydrodynamics to glacial forcing, including its seasonality. Also, it is one of the first attempts to model a 3D circulation within a glacial bay with multiple glaciers, showing relative significance of different forcing mechanisms and allowing inferences about their impact on local ecosystem and on the Southern Ocean system in general.

2 Study area

Admiralty Bay is a large inlet of King George Island (KGI), the biggest island in the South Shetlands (Fig. 1 a), a region described as especially sensitive to climate change (Bers et

al., 2013). The acceleration of glacial melting during summer (Rückamp et al., 2010) and the recent absence of sea ice during winter are the most prominent indicators of this vulnerability (Eayrs et al., 2021; National Snow and Ice Data Center, 2023).

KGI is covered in 90% with ice, divided into interconnected icecaps (Simões et al., 1999). Twenty-five percent of AB's 150 km long coastline consists of ice–water boundaries, formed by twenty maritime glaciers draining directly into the bay waters (indicated with orange lines in Fig. 1 b). All of them are relatively shallow (Fig. 1 c.), with an estimated maximum grounding depth of ~150 m, and the majority of glacial fronts submerged by less than 50 m. Because of that, AB glacial fronts are considered to be nearly uniform vertically, without evidence for undercutting or floating tongues (Carroll et al., 2016). AB glaciers can be classified as intermediate forms between polar and temperate glaciers, with both geothermal and frictional heating as well as external warming inducing water discharge into the ocean (Jenkins, 2011). A comparison of a regional map from 1990 and recent satellite imagery (Battke, 1990) shows a significant retreat of local glacier fronts over the past 31 years.

Additional freshwater input into the bay is produced by glacial creeks, which frequently carry waters from glaciers that have recently retreated to land. Their existence and the amount of water being supplied through them vary significantly throughout the year. Consistently reoccurring summer creeks (17 separate outlets) noted by (Potapowicz et al., 2020) and observed by the crew of the Arctowski Polish Antarctic Station have been marked in Fig. 1 b. with red points. The mean annual precipitation in AB adds up to around $6.75 \cdot 10^7$ m^3 (Plenzler et al., 2019), whereas glacial input to $6.3 \cdot 10^8$ m^3(estimation based on a conservative assumption of outflow of 20 m^3/s; see sections 4.2 and 5 for details). Therefore, the impact of freshwater from precipitation was not considered in this analysis.

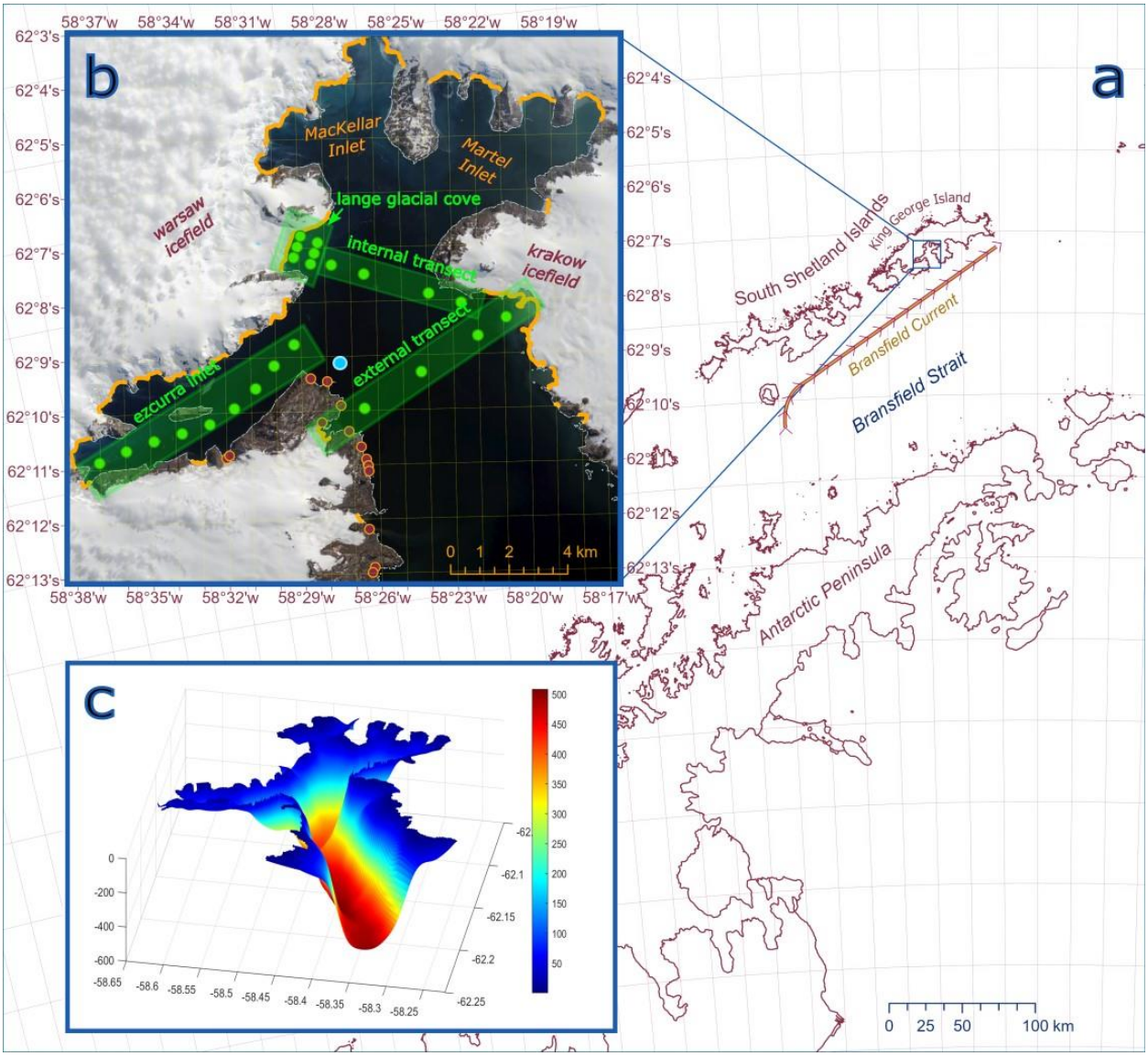

Figure 1. Admiralty Bay. **a.** regional map (Gerrish et al., 2021), Bransfield Current is marked as per (Thompson et al., 2009); **b.** ocean-ice boundaries (Gerrish et al., 2021) and known creek outlets (Potapowicz et al., 2020 and observations), marked with orange lines and red dots, respectively. Green points show *in situ* measurement sites and green boxes their groupings. Blue dot indicates wavemeter mooring location (inset based on Sentinel imagery, 29.12.2021); **c.** AB bathymetric map (in meters).

AB has an area of 135 km^2 and has been previously described as a wide fjord, however, geomorphologically, it is a tectonic estuary (Valle-Levinson, 2010), formed by geological faults (Majdański et al., 2008), which explains its distinction from northern hemisphere fjords. For the purposes of this study, a new, hitherto most precise bathymetric map of AB has been created, compiling data from (Battke, 1990; Magrani et al., 2016; Majdański et al., 2008) and self-conducted ADCP measurements (Fig. 1 b). It shows that AB's mean depth is 160 m, but in its central part there is a relatively narrow trough up to 600 m deep. AB is connected with Bransfield Strait through a 8 km wide opening, notably, without a well-defined sill.

Tidally controlled water level shifts oscillate between –1.5 and 1 m at the AB outlet (Padman et al., 2002). Locally, the most common wind direction is SW, present for around 25% of the time; wind events from other directions take up from 5 to 10% of the time (Plenzler et al.,

2019). The occurrence frequency of long-lasting periods of along-fjord (NW or SE) katabatic winds, controlling water exchange with the ocean is, low. This is in contrast to Greenland, as noted by (Spall et al., 2017). Nevertheless episodic occurrence of this process is possible as recorded, e.g., in Andvord Bay by Lundesgaard et al. (2019).

In Bransfield Strait, Bransfield Current flows in a northeastern direction along the southern border of the South Shetlands and creates an effective barrier from outside currents (Moffat & Meredith, 2018; Poulin et al., 2014; Zhou et al., 2006); see Fig. 1 a). This blocking mechanism is strengthened by local bathymetry, which, close to the AB outlet, drops rapidly to over 2000 m, so that relatively shallow AB-shelf waters are only to a limited extent influenced by deep ocean hydrodynamics. Consequently, currents impacting the AB directly are forced by tides, with the Coriolis force playing a key role, which together drive full water exchange between the AB and the ocean in estimated 147 hours (Zhou et al., 2020).

3 Hydrographic measurements

3.1 Methodology

Since December 2019, a comprehensive *in situ* measuring campaign has been conducted using YSI Exo CTD+ sondes to investigate the AB water properties. The openly accessible data up until January 2022 can be found in the PANGAEA repository (Osińska et al. 2022). Detailed information regarding the scope and methodology of data collection is described in Osińska et al. (2023). Measurements conducted using an unaltered methodology have continued up until February 2023, and their findings have been analyzed in this study. This dataset has high resolution in both time and space. For the present analysis, 23 measurement sites with depths exceeding 10 m were chosen (Fig. 1 b; green points) and divided into four zones (Fig. 1 b; green boxes):

- *external transect* – central region of AB's main body, in closest proximity to the open ocean,
- *internal transect* – further within the bay yet still within the main body of AB,
- *Ezcurra Inlet* – within the smaller western inlet of AB,
- *Lange glacial cove* – sites less than 1 km away from the medium-sized Lange glacier

Measurements with missing salinity records and from the top 0.5 m of the water column have been excluded from the analysis (due to high uncertainty of near-surface measurements). A time-averaged salinity profile ($S^x(z)$) was calculated for each site from all measurements at that site $s_n^x(z)$, where *z* denotes depth, *x* denotes a specific site and *n* is an index of individual measurement at that site. The following records have been classified as outliers and removed from the dataset:

- 5% of profiles at each site with the largest standard deviation of differences (σ_D) from that site's mean salinity profile
- 5% of profiles at each site with the largest difference between vertically-averaged $s_n^x(z)$ and vertically-averaged $S^x(z)$

After this procedure, the remaining dataset consisted of 1830 profiles from 136 days and all seasons of the year.

Freshwater thickness (FWT) was determined for all profiles using the Holfort et al., (2008) formula:

$$\mathrm{FWT} = \int \left(\frac{S_{ref} - s_n^x(z)}{S_{ref}}\right) dz \qquad (1)$$

where S_{ref} is a reference salinity value. S_{ref} was determined for each measurement day as the mean salinity value from all measurements from that day below 60 m. The decision to use records from below 60 m was based on modeling results that showed glacial water spreading maximally to this depth (details in Section 4.3.2).

3.2 Results analysis

Fig. 2 provides a comprehensive depiction of the fluctuations in AB water properties over four years of hydrographic measurements. Overall, the water temperature varied in a range of –2 to 2˚C, while the salinity ranged from 33.3 to 34.6 PSU (Fig. 2 a–h). The temperature and salinity fluctuations in AB exhibited a high degree of spatial homogeneity. This is evidenced by the similarity in temperature changes throughout different parts of AB depicted in Fig. 2 a, c, e, and g. Similarly, the salinity changes shown in Fig. 2 b, d, f, and h also displayed a consistent pattern. Notably, the average salinity values observed in the *external transect* were lower than those observed in other regions. Upon closer examination of the individual sites within the *external transect* (Fig. S1) it becomes evident that the aforementioned pattern is mostly attributed to the low salinity values observed at the two eastern sites. Conversely, the salinity values at the two western sites exhibit a comparable or higher range to the values depicted in Fig. 2 b, d, f, and h. Despite differences in salinity values, the water temperature fluctuations at all *external transect* sites are similar.

The freezing line seen in TS diagrams (Fig. 2 j-m) shows that most of the time AB water properties were well above freezing conditions during all seasons of the year (details in Osińska et al., 2022). This is the reason for the absence of winter sea ice coverage in AB over the course of the measuring campaign.

The freshening of AB's surface water during warm months (Fig. 2 b, d, f, and h) and the corresponding peaks in FWT (Fig. 2 i) indicate the presence of GMW. This is because marine terminating glaciers are a primary source of freshwater in the northern WAP region, as established by (Powell & Domack, 2002). Additionally, it has been determined that the contribution of sea ice and precipitation to AB's freshwater content is limited. No evidence of fresher water plumes in subsurface layers was detected (Fig. 2 h and more details in Osińska et al., 2023). Hence, the GMW continuously exhibits the highest buoyancy among the water masses in the AB region, a finding that has been corroborated by prior investigations conducted in the area (Meredith et al., 2018; Monien et al., 2017; Osińska et al., 2021).

TS diagrams, as shown in Figure 2 j-m, are used to differentiate between water masses inside of the AB. AB waters during the winter are generally homogenous, with temperature and salinity marginally rising as depth increases. During the spring season, a fresher and warmer layer of water is formed on the surface, overlaying waters characterized by increasing salinity and temperature with depth. Two layers in the AB water column are also present during summer and autumn. The summer surface layer experiences maximum freshening (average salinity dropping to 33.2 PSU) and warming (mean temperature ranging from 1 to 1.5 degrees Celsius).

During the autumn, the upper layer, in comparison to the summer season, exhibits lower temperatures and higher salinity.

In conclusion, it has been shown that AB contains up to two characteristic water layers throughout the course of a year. The distribution of these layers' salinity and temperature values can be largely attributed to atmospheric and glacial influences. The water mass found below the surface layer during the seasons of spring, summer, and autumn, as well as the principal water mass observed during winter, shall be referred to as ambient water (AW). This water mass is primarily impacted by the waters of the Bransfield Strait and by atmospheric forcing. AW exhibit relatively small variability throughout the year and display typical patterns of seasonal fluctuation commonly observed in estuarian deep waters (Cottier, et al., 2010). Fresh surface waters found in spring, autumn, and particularly during the summer are classified as GMW. GMW consists of a mixture of AW and glacial water that originates from subglacial discharge, submarine melting, glacial creeks, and icebergs. These waters are heated and cooled to varying extents through atmospheric forcing. The lowest summer surface temperatures were recorded in *Lange glacial cove* since the freshly formed GMW surface layer has a limited duration of atmospheric exposure. Notably, there is a possibility of external freshwater entering AB at the surface, which may be indistinguishable from GMW using solely salinity records.

The presence of warm and highly saline Atlantic Waters in Greenland (Sciascia et al., 2013; Slater et al., 2018; Straneo et al., 2011) and CDW in the Antarctic (Cape et al., 2019; Moffat et al., 2009) has been shown to directly stimulate glacial melting and play an important role in shaping the hydrodynamics of glacial bays. The hydrographic data analyzed here does not support the existence of such warm external water masses in AB. The measurements conducted in this investigation were limited to a maximum depth of 100 meters. Consequently, it is possible that distinct water masses could infiltrate deeper AB waters and remain undetected. Nevertheless, the probability of such an event and its substantial influence on AB's glacial-oceanic boundary is low. Because water depth near AB glaciers seldom exceeds 100 m (Figure 1 c), any warmer and more saline water intrusions would be unable to reach glacial fronts unless their presence were recorded at shallower measurement sites. Additionally, earlier measurements conducted in AB over a wider vertical range also did not find any signs of the presence of such water masses (Carbotte et al., 2007). Finally, studies of regional ocean circulation concluded that CDW intrusions into AB are unlikely (Hofmann et al., 2011; Sangrà et al., 2011).

The general two-layered stratification enables the determination of the internal Rossby radius, which serves as a metric for evaluating the relative significance of water column stratification in comparison to rotation (Cottier et al., 2010). In the AB, depending on conditions, the internal Rossby radius varies between 0.41 and 11.86 km and compared to the ~8 km wide opening, it indicates that the AB can be classified as a "broad bay", where the presence of cross-

bay circulation has substantial importance.

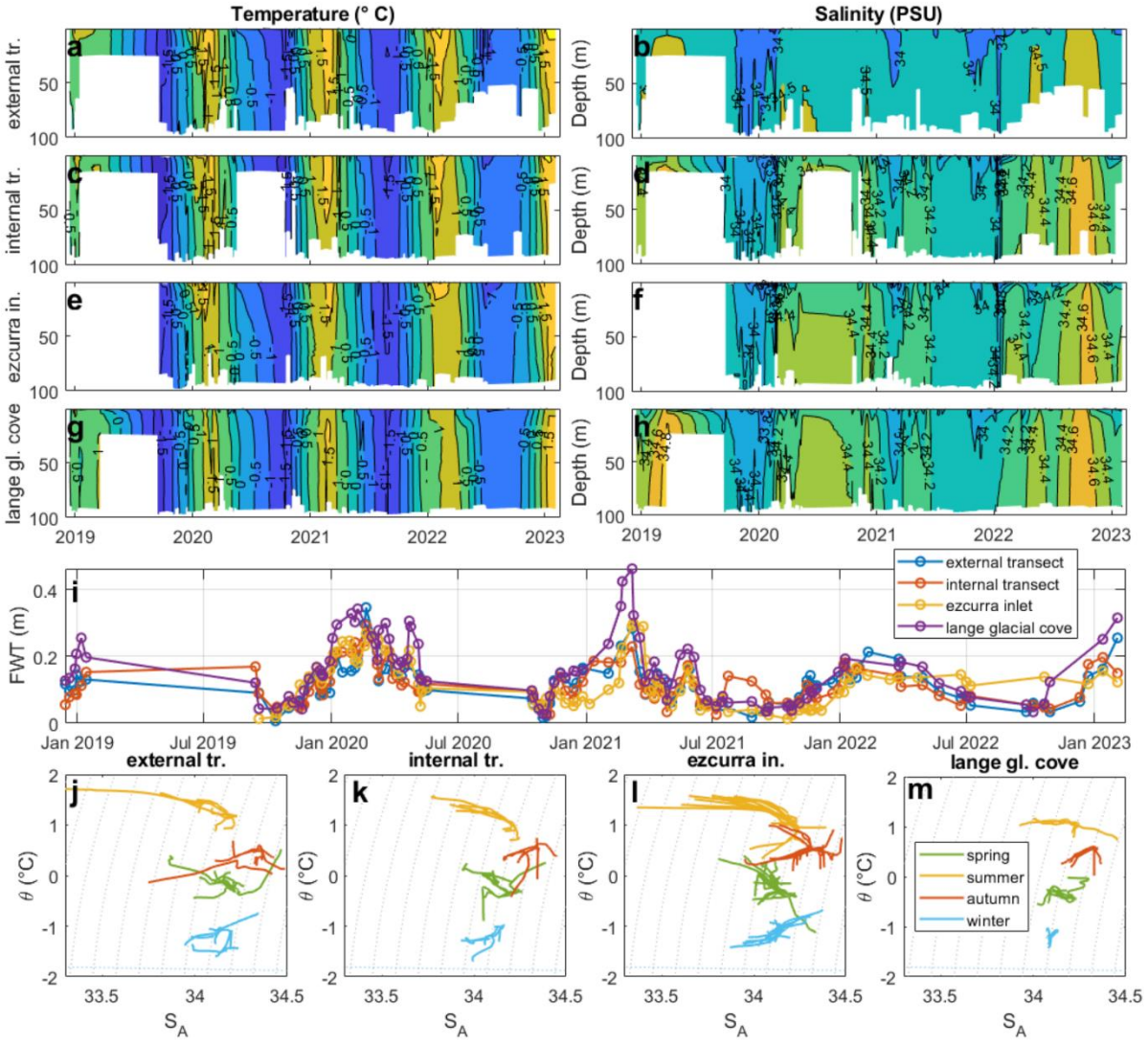

Figure 2. Overview of salinity and temperature records in AB. **a,c,e** and **g** mean temperature (˚C) and **b,d,f** and **h** mean salinity (PSU) in four zones: **a-b** – external transect, **c-d** internal transect, **e-f** Ezcurra inlet, **g-h** Lange glacial cove; **i** –mean freshwater thickness (m) from all sites in different zones; **j-m** TS diagrams of mean seasonal values from each site, blue dotted line – freezing line.

4 Hydrodynamic modelling

4.1 Model setup

The presence of a two-layered stratification in AB, where the surface layer consists of the most buoyant layer of glacial meltwater (GMW), is reminiscent of the conditions outlined in the small-fjord single-cell circulation model proposed by (Motyka et al., 2003). However, due to the "broad" character of the bay, the AB model must be three-dimensional.

Modelling of AB hydrodynamics has been performed using the open-source Delft3D-Flow model, developed as part of a Delft3D suite created specifically for coastal, river, and estuarine hydrodynamics (Deltares, 2020). The calculations were performed on a high-resolution

curvilinear grid of over 30,000 points, thus, an average grid cell corresponds to an area of approximately 55 m^2. The analysis was conducted in 3D, with fifty layers utilizing a vertically scaled σ-coordinate system, with more densely spaced layers toward the domain's bottom and top. The bathymetric map shown in Fig. 1 c was used with a single smooth, ~10 km long open boundary between AB and Bransfield Strait.

The model was driven by tides, and temperature and salinity gradients. The tidal water level at the open boundary was calculated using the CATS2008 Antarctic tides model (Padman et al., 2002). Temperature and salinity data reanalysis by Dotto et al. (2021) was used to determine temperature and salinity values at the open boundary since it is the most robust data source for water properties in the northern WAP region, combining the majority of available *in situ* measurement records from 1990 to 2019. Seasonally averaged (for spring and summer) reanalysis values were extracted from a grid point closest to the model's open boundary and interpolated in time and space to create varied vertical salinity and temperature profiles. Dotto et al. (2021) results show that Bransfield waters are weakly stratified (Fig. S2) with seasonal mean temperature and salinity variations of -1.23–0.51˚C and 34.22 –34.27 PSU. The *in situ* measurement results from Osińska et al. (2023) were used to determine initial values of water salinity and temperature inside AB, which were uniformly set throughout the domain. It has been found during preliminary model testing that after less than three days of simulations, the salinity stratification in the whole bay was predominantly influenced by the open boundary input, therefore no variation in the initial conditions setting was necessary.

To capture the variability associated with the entire range of tidal patterns in this region, calculations lasted 58 days (from 1.12.2021 to 28.01.2022), consisting of 3.5 days of model warm-up followed by two full lunar cycles.

Following Deltares recommendation, bottom roughness was calculated using the 3D Chézy formula (Deltares, 2020), and assumed spatially homogenous due to lack of information on bottom roughness variations in AB. During model testing, it was discovered that unreasonably high values of energy dissipation (>1000 m^2/s^3) were obtained close to the open boundary after approximately two days of calculations and persisted throughout the simulation length. It was determined that this was caused by inappropriately assessed bottom roughness. Through several additional test runs it was experimentally found that uniform 3D Chézy bottom roughness coefficients of 40 $m^{1/2}/s$, in both U and V directions, is the highest coefficient value which does not result in unrealistic energy dissipation anomalies, which cause a rapid increase in flow velocities near the open boundary, and consequent model destabilization. Hence, this value was regarded as appropriate and was used in all subsequent calculations.

Additional information regarding the model configuration can be found in Table S1. Importantly, as indicated by the aforementioned description of the model configuration, no atmospheric forcing was considered, i.e., ocean-atmosphere momentum, heat, and moisture fluxes were set to zero. This decision is justified by the fact that, first, the salinity differences between the oceanic and glacial waters dominate the density structure and gradients in the domain of study, and second, volume fluxes associated with tidal currents dominate those generated by wind, particularly over the time scales of several tidal cycles considered here. Such simplification is not unusual in studies at this scale (Straneo et al., 2011).

The typical density anomaly of water entering through the open boundary and that of the meltwater is σ=27.4 kg/m^3 (at S=34.1 PSU and T=–0.2 ˚C) and σ=0 kg/m^3 (at S=0 PSU and

T=0˚C), respectively. The highest recorded value of surface water temperature observed in AB in the summer was 3.54 ˚C, which was exceptionally high (Osińska et al., 2023); the corresponding density anomaly at S=32.56 PSU is σ=26.0 kg/m^3. Therefore, the contribution of temperature to the net variability of water density in AB is minor. Accordingly, the core of the analysis and discussion in the following sections is considering factors driven by salinity fluctuations. Since seasonal salinity variations derived from Dotto et al. (2021) dataset are small (<0.1 PSU difference between mean seasonal values) model setup accurately replicates AB open boundary conditions throughout the year.

For model validation purposes, an RBR wavemeter was moored within Admiralty Bay (location indicated with blue dot in Fig. 1 b) logging water level at 2 Hz frequency during the period from 6.12.2021 to 21.12.2021. The standard deviation of differences between Delft3D model data at this location and *in situ* RBR measurements is 0.08 m, the bias is 0.03 m, and their correlation coefficient is 0.99, i.e., the modeling results correspond very closely to the real water level changes in that part of AB. Analogously, CATS2008 compared with RBR measurements has a 0.08 m standard deviation of differences, a bias of 0.01 m, and correlation coefficient of 0.99 (see Fig. 5 a).

4.2 Location, dispersal and volume of glacial freshwater influx

The representation of interactions between glaciers and oceans is a crucial component in establishing the framework for glacial bay hydrodynamical modelling. The description of oceanic dynamics near marine terminating glaciers often relies on the buoyant plume theory (BPT). The BPT explains how freshwater discharged from underneath the glacier upwells along the glacial front, entraining and mixing with ambient waters to form a GMW plume. This plume then induces the submarine melting of the glacier's front (Jenkins, 2011). The submarine melt rate is influenced by subglacial discharge volume and ambient water temperature, however, this relationship varies depending on the study location (Kimura et al., 2014; Sciascia et al., 2013; Xu et al., 2012). When GMW reaches its depth of neutral buoyancy, which may occur at or below the ocean surface, it forms a layer of distinct properties within the water column (Jenkins, 2011). The influence of glacial water on ocean hydrodynamics is contingent upon the distribution of subglacial discharge points, namely whether they are channelized or uniformly distributed along the glacial front, and the momentum of the discharge (Cowton et al., 2015; Slater et al., 2018).

The Buoyant Plume Model (BPM) coupled with the general circulation model (GCM) is currently considered the most sophisticated method for investigating the hydrodynamics of glacial bays (Cowton et al., 2015). However, its application may not always be necessary or practical. In an earlier investigation conducted by Chauché et al. (2014) observational data indicated that subsequent to channelized release, subglacial influx rapidly spreads laterally along the glacial front, effectively blurring the distinction between effects of localized and uniformly dispersed freshwater injection points. The study by Sciascia et al. (2013) demonstrated that the hydrodynamics of near-glacial waters is influenced to a greater extent by the volume of subglacial discharge than the momentum of its inflow. The usage of the BPM coupled with GCM for the purpose of modeling the hydrodynamics of bays with multiple ice-water boundaries is challenging. Firstly, such multiway coupling is computationally expensive. Furthermore, it requires detailed bathymetric and glaciological data, including discharge location points, volumes, and submarine melt rates (Carroll et al., 2016) which is currently unattainable in AB and, we argue, in the majority of glacial bays in Antarctica.

In light of the practical challenges involved, a question arises regarding the extent to which accurately reproduced vertical location and velocity of glacial water influx is significant for the understanding of general AB hydrodynamics. In order to address this question, several iterations of model tests were conducted, in which glacial water discharge locations and velocities were varied. The following are the identifiers and details of these test runs:

- *H0* - test run with glacial water discharged from all glaciers, homogenously through the entirety of glacial front, with zero initial velocity (treated as reference case for other scenarios)
- *H2* - test run with glacial water discharged from all glaciers, homogenously through the entirety of glacial front, with an initial velocity of 2 m/s
- *S0* - test run with glacial water discharged from all glaciers subglacially, with zero initial velocity
- *S2* - test run with glacial water discharged from all glaciers subglacially, with an initial velocity of 2 m/s

In order to emphasize the potential influence of glacial discharge velocity on AB hydrodynamics, a high value of 2 m/s was selected for testing (Cowton et al., 2015; Xu et al., 2012). The volume of the glacial discharge for all test runs was established at ~6 m^3/s per 1 km of glacial front, a value that was deemed reasonable for the AB region during the summer melt season (see section 5).

Three measures were employed to examine disparities between test run results: FWT (Figure 3 a-d), pycnocline depth (Figure 3 e-h), and depth-averaged flow velocity (Figure 3 i-l). These metrics serve as the foundation for further analysis of AB hydrodynamics, making them suitable instruments for determining if the results of test scenarios exhibit substantial differences between each other. FWT was calculated using formula (3), where S_{ref} was determined as the mean salinity from below 60 m across the entire AB. Given the stratification of model open boundary waters, the utilization of this FWT calculation method shows the presence of freshwater influx from the Bransfield Strait into AB. Hence, in order to illustrate the distribution of freshwater originating exclusively from AB glaciers, the FWT values calculated for a scenario devoid of glacial water inflow (scenario *0 m^3/s*) were subtracted from the FWT results of the four test runs. The pycnocline depth was calculated as the depth at which $d\sigma/dz < 0.025$ kg/m^3. The data that have been analyzed and presented in Fig. 3 were averaged over a period from January 1st, 2022 to January 28th, 2022, which corresponds to a one complete lunar cycle.

All test run results show consistent patterns in the FWT, pycnocline depth, and flow velocity values distributions across the AB (Fig. S3). On the other hand, discrepancies are visible when comparing maps of differences between test runs and the reference case *(H0)* results (Fig. 3).

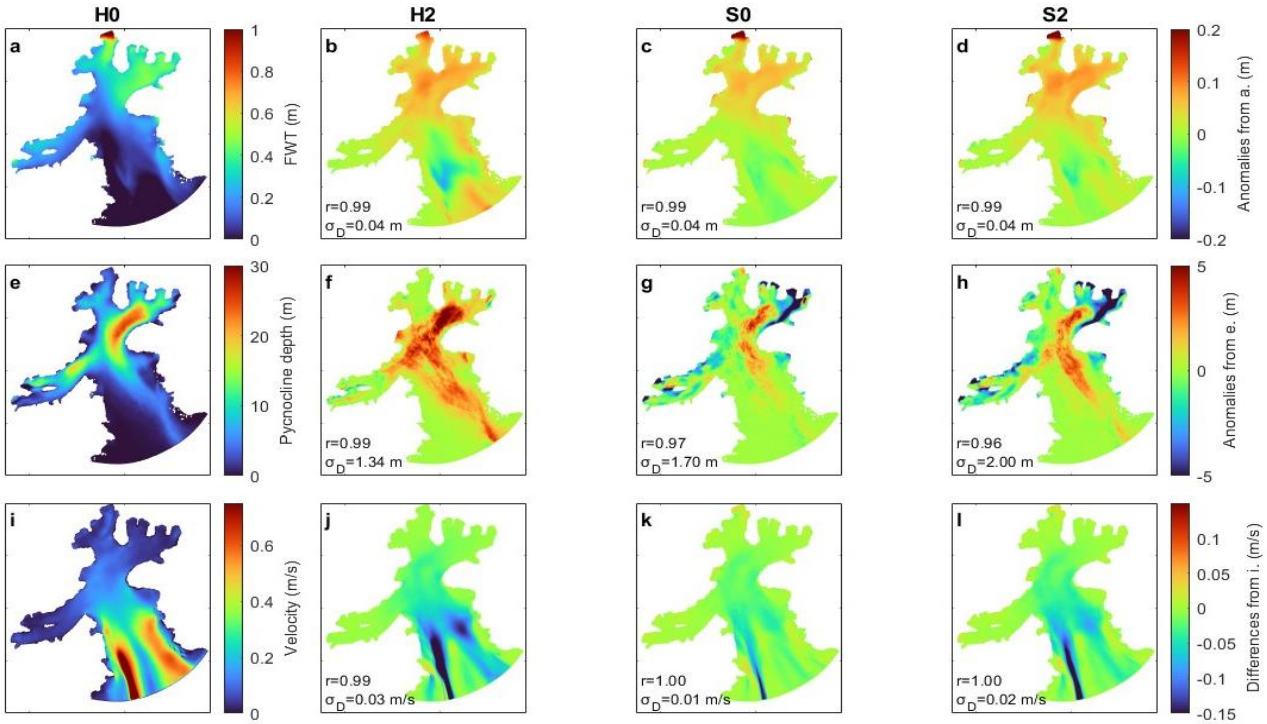

Figure 3. Comparison between model results with different glacial discharge locations and velocities. **a-d** FWT (m); **e-h** Pycnocline depth (m); **i-l** depth averaged velocities in m/s; **a,e** and **i** H0 scenario – reference case; **b, f** and **j** H2 scenario differences from the reference case; **c,g**, and **k** S0 scenario differences from the reference case; **d,h** and **l** *S2* scenario differences from the reference case. $\boldsymbol{r}$, $\boldsymbol{\sigma_D}$– correlation coefficients and standard deviation of differences between shown results and reference case respectively. All figures depict mean values from period from 1.01.2022 to 28.01.2022.

For all test scenarios the FWT values are highest in the northwest region of AB, ranging from 0.35 to 0.55 m, (Fig. 3 a-d). In that area the three scenarios *H2*, *S0*, and *S2* have slightly greater FWT values (<0.1 m) than the reference scenario *H0*. The overall FWT differences between scenarios range from −0.1 to 0.15 m (Figure 3 b-d). In test runs with solely subglacial discharge, narrow regions of elevated FWT form along glacial fronts. The biggest differences in FWT and pycnocline depth are observed in scenario *H2* (Fig. 3b and f). For instance, in an area of a maximum pycnocline depth (~25 m) for *H0*, the pycnocline depth increases by up to 4 meters in *S0* and *S2*, and by over 6 m in *H2*. In *S0* and *S2* scenarios the presence of subglacial discharge and subsequent turbulent mixing prevents pycnocline formation in regions close to glacial fronts (blue areas in Fig. 3 g and h). Crucially, the overall flow pattern remains consistent in all examined cases, characterized by a strong influx from Bransfield Strait along the AB's western bank and an outflow in the east (see more details in section 4.3.2). The differences in flow velocities, shown in Figure 3 i-l, are largest close to the AB opening. In scenarios *H2*, *S0*, and *S2*, the AB's inflow and outflow have reduced velocities compared to the reference case results. This slowing down is largest in cases in which glacial waters are discharged with 2 m/s velocity (up to a −0.25 m/s decrease in *H2* and −0.15 m/s decrease in *S2*).

The model test run results show that the freshwater content, the water column stratification, and the flow velocities in AB are locally impacted by changes in the location and momentum of glacial influx. In general, larger differences in the analyzed metrics were caused by variations in the velocity of glacial input rather than an alteration in its vertical position. Nevertheless, the overall circulation and glacial freshwater distribution patterns in AB have not

changed as a result of employing any of the studied model configurations (Fig. S3). This conclusion is further strengthened by the high correlation coefficients (r) and low σ_D for all employed metrics across all scenarios (Fig. 3). Therefore, it i justified to conclude that for examining the overall impact of glacial water on AB hydrodynamics, a simplified methodology that disregards the influence of the vertical position and velocity of glacial injections is adequate.

Consequently, further model simulations were performed with glacial water discharged homogenously through the entirety of the glacial front, from all glaciers, with zero initial velocity. A total of fourteen scenarios with increasing volumes of glacial runoff were calculated: 0, 0.15, 0.3, 0.6, 0.9, 1.7, 3.0, 4.5, 6.0, 8.0, 11.0, 14.0, 28.0, and 60.0 m^3/s of freshwater volume discharged per ~1 km of glacial front. Henceforth, these values will be employed as identifiers for the scenarios in order to enhance the conciseness and clarity of the text. Input of freshwater from the creeks was assumed to be vertically homogenous, was of equivalent volume to runoff from ~1 km of a glacial front in a given scenario and was introduced through a single grid cell.

4.3 Response of AB hydrodynamics' to the increase in glacial discharge

4.3.1 Water level changes

Modeling results were analyzed through Principal Component Analysis (PCA) of water levels, using results from two full tidal cycles from 4.12.2021 12:00 to 28.01.2022 00:00. Each PCA mode consists of a spatial distribution (map) of PCA coefficients (also known as loadings), a time series of PCA scores showing the relative strength of that mode through time, and the overall percentage of the total variance of the dataset explained by that mode. Through the calculation of the squared correlation coefficients (r^2) between scores of PCA modes and time series of water level in all active grid points, maps of the spatial distribution of percentages of variance explained by the first four modes have been obtained (Fig. 4 b-e).

Water level changes in AB are uniformly and almost exclusively driven by tidal shifts. This is demonstrated in Fig. 4 a. where a comparison of *in situ* measurements collected by RBR wavemeter moored 9.5 km away from the AB outlet (location marked in Fig. 1 b) with tidal data from CATS2008 at the open boundary of the Delft3D model is shown. The blue line corresponding to *in situ* measurements exhibits only small deviations from modeled data, presumably during periods of very strong winds. The yellow line represents Delft3D model results at the grid point closest to the wavemeter location. The very good agreement between the three curves shows that the water level in the whole AB reacts almost instantaneously to the open boundary forcing.

PCA analysis of water level in the *0 m^3/s* scenario further confirms almost instantaneous response of the whole AB to tidal shifts. Fig. 4 b-e shows maps of coefficients corresponding to the first four PCA modes and the percentage of water level variance explained by them, respectively. The first PCA mode (PCA 1), which represents homogenous changes in the water level of the whole AB, explains more than 99.8% of the variance in all studied scenarios. Accordingly, the PCA 1 score correlates almost perfectly with the time series of water level at the boundary and inside of the model domain (see time series in Fig. 4 a). This indicates that anomalies from this pattern are of the order of a hundredth of a percentage, even in the *60 m^3/s* scenario, in which an additional 2000 m^3 of water is pumped into AB every second. The predominance of tidal impact on water level changes is not surprising, since volume flux through the open boundary is of the order of 100 000 m^3/s.

Although explaining small percentages of variance, other PCA modes of water level shifts are showing important characteristics of water level fluctuations in AB. Modes 2-4 represent standing-wave-like water level fluctuations with respectively one, two, and three nodes (Valle-Levinson, 2022). Each of the maps in Fig. 4 b-e emphasizes a region in central AB that corresponds to the location of a smaller circulation cell in the overall AB circulation pattern (Section 4.3.2 and Fig. 5).

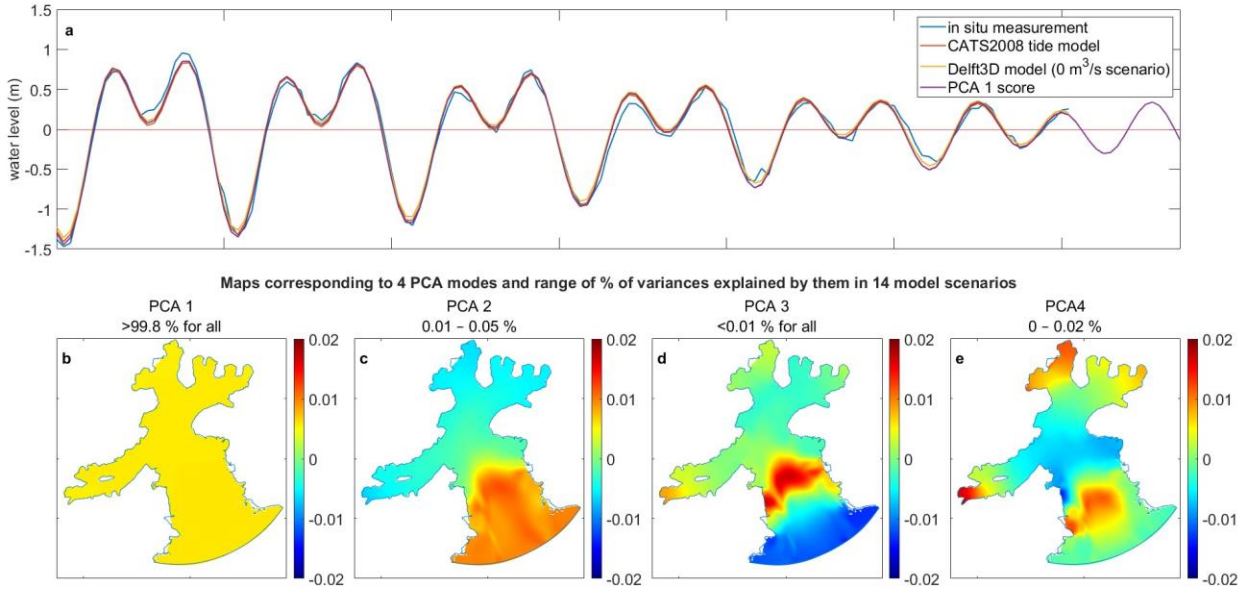

Figure 4. Results of PCA analysis of water level changes in 14 scenarios. **a.** comparison of in situ water level measurements, CATS2008 tide model input data, Delft3D 0 m^3/s model results and normalized PCA1 score (note that score values are non-dimensional, they have been divided by its double standard deviation to fit); **b-e** maps corresponding to first four principal components of water level 0 m^3/s scenario (-); the percentages of water level variance explained by each mode in fourteen scenarios are shown above each map.

4.3.2 Changes in circulation and freshwater distribution

The most notable feature of AB general circulation is a strong northerly flow along its western boundary (Fig. 5 a.). It is formed by the Coriolis force acting upon Bransfield Strait waters flowing northeast along the edge of the South Shetland Islands (Zhou et al., 2002). The existence of this current was recognized by prior modeling conducted in the AB by (Robakiewicz & Rakusa-Suszczewski, 1999). Following its initial development, the AB inflow current continues in a northerly direction and subsequently undergoes bifurcation. Part of it flows to the right in the central region of the main body of the AB, approximately 7 kilometers from the AB outlet (around the location of *main AB* cross-section), and then exits the bay in close proximity to its eastern boundary. The second limb of the current penetrates deeper before reversing its course in the main embranchment of the bay (~13.5 km from the opening) and also flows back to the bay opening along its eastern coast. The clockwise (cyclonic) circulation cells formed by these two branches are crucial elements of the water exchange mechanism between the ocean and inner bay waters. A visualization of monthly average velocities across the *main AB* cross-section (Fig. 5 b) reveals that this exchange has the greatest magnitude in the surface layer. In the scenario without glacial influx there exists a state of equilibrium between the amount of water flowing into AB via its western half and the amount flowing out of it through the eastern

half of the *main AB* cross-section (Fig. 5 f). At spring tide, the volume of water transported through each of the halves reaches 2 * 10^5 m^3/s. The quantities of water penetrating the three inner inlets of AB, Ezcurra, MacKellar, and Martel Inlet are two orders of magnitude smaller, with proportionally lower velocities observed across their respective cross-sections (Fig. 5 c-e, and Fig. 7 z-cc).

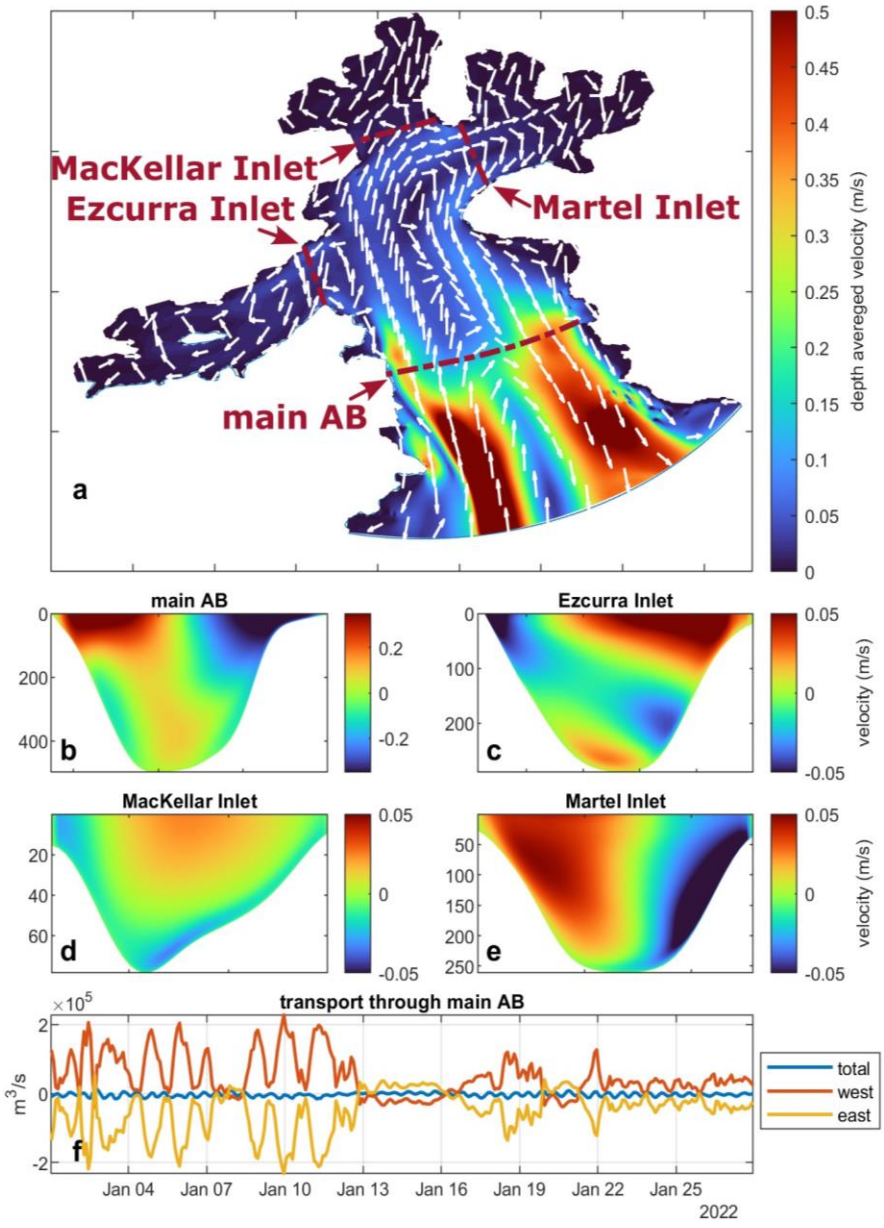

Figure 5. General circulation pattern of AB in without glacial influx ; **a**. flow depth averaged velocities (map colors) and directions (white arrows); **b-e** velocities across four crossections (their location in Fig. 6 a.), positive values correspond to inflow into bays, negative to outflow; **f.** transport through main AB crossection, total (blue line) and divided into western (red line) and eastern half (yellow line). Values in a-e are average for the period 1.01.2022-28.01.2022.

When glacial influx is introduced, AB's cyclonic circulation explains the development of distinct patterns in glacial water dispersal, illustrated by FWT and pycnocline depth maps (Fig. 6). In each of the model scenarios, following an initial warm-up period, a quasi-stationary state is reached, in which the distribution of FWT remains approximately constant (Fig. S4). With rising

glacial influx levels, freshwater accumulates in the northeastern region of AB, specifically in MacKellar and Martel Inlets. This freshwater is then transported to Bransfield Strait by the AB's eastern outflowing current. In the accumulation zones, the FWT values range from 0 to 0.5 m. The FWT exceeds 1 m in larger areas only in the two strongest glacial influx scenarios, *28 m^3/s* and 60 *m^3/s*. The increase of glacial input results in the expansion of the region where the pycnocline occurs, as well as in its deepening. The pycnocline depth is determined by the local bathymetry, resulting in the deepest pycnocline developing in the area of the main AB embranchment. In all scenarios, the depth of the pycnocline does not exceed 60 meters.

The model results demonstrate circulation and freshwater distribution patterns that are consistent with the *in situ* measurement data. The average salinity values from the top 60 m of water at two sites in the western inflow area, *ve6* and *ez9*, consistently exceed those reported at the outflow sites, *ve4* and *lv3*. Despite the close proximity and similar distance from the glacial front and bay's outlet between inflow and outflow sites, this salinity difference can reach 0.3 PSU (Figure 6 u. and Figure 6 a. for site location and Fig. S1).

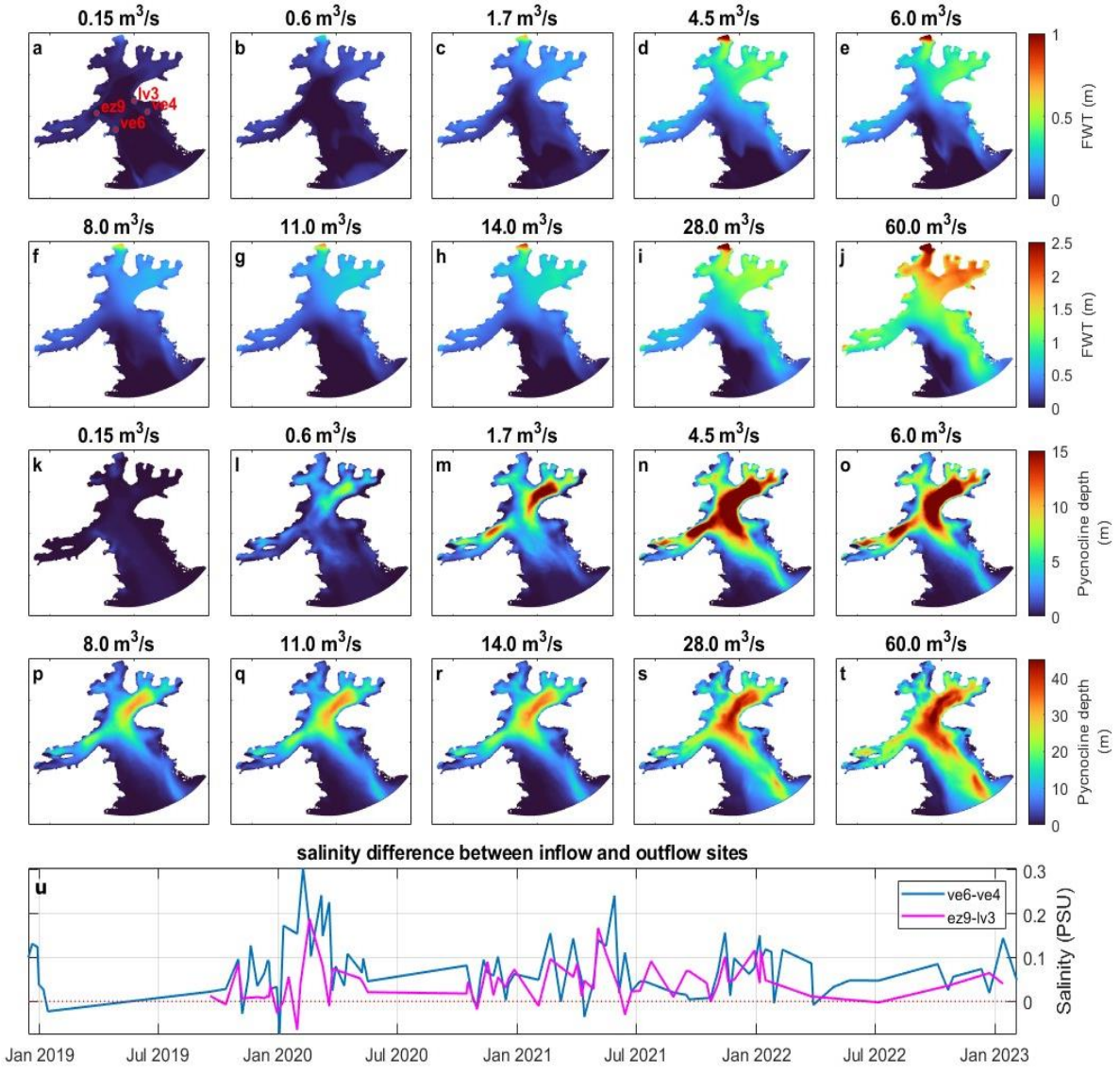

Figure 6. Variability of FWT and pycnocline depth with increasing glacial input; **a-j** FWT; **k-t**. pycnocline depth. Note changing scales in different rows; **u**. difference in average salinity readings from top 60 m of inflow (ve6 and ez9) and outflow (ve4 and lv3) sites (sites' locations seen in a.) Values in a-t are average for the period 1.01.2022-28.01.2022.

In all the model scenarios, the circulation pattern of two cyclonic circulation cells is preserved in AB (Fig. 7 a-e). The analysis of flow velocities and transport volumes across the *main AB* cross-section reveals that in scenarios ranging from *0* to *14 m^3/s*, the water exchange is consistently strongest near the surface and has a volume of ~10^5 m^3/s for both inflow and outflow (Fig. 7 f-j, and Fig. 7 z, analogous to Fig. 5 b and 5 f). However, in two highest glacial influx scenarios (*28* and *60 m^3/s*), the water transport on both sides of the main AB cross-section decreases significantly to ~10^4 m^3/s (Fig. 7 z). Similarly, in these scenarios, the flow velocities are reduced (see Fig. 7, e and j). This observation suggests that a threshold value of glacial inflow volume exists limiting water interchange between the bay and the ocean. Specifically this threshold is observed to be between *14* and *28 m^3/s* ~1 km of glacial front, which adds up to 450 and 900 m^3/s of overall freshwater input into AB.

In cross-sections located at the openings of inner AB inlets, Ezcurra, MacKellar, and Martel Inlets, the impact of increasing glacial influx is visible from relatively low glacial water inflow rates below 0.6 m^3/s, (Fig. 7 f-y). The surface outflow layer forms there, moving GMW out of the bay, most evidently in the Ezcurra and MacKellar Inlets (Fig. 7 k-t). Fig. 7 aa-cc. shows the variability in water volume transported through the three inlet cross-sections in 14 model scenarios, in total, and split into layers above (surface layer) and below the pycnocline depth (calculated as in section 4.2). In AB inlets, surface outflow and deeper inflow increase with rising glacial influx, up to *14 m^3/s* scenario, when their values stabilize. This demonstrates how glacial influx drives vertical circulation, similar to the 2D glacial bay circulation of (Motyka et al., 2003). The drop in total transport values in Fig. 7 aa-cc indicates the importance of additional freshwater input for the water budget of AB inner inlets, which is barely visible in the flow transport sum up through the *main AB* cross-section, where overall values are 100 times higher (Fig. 7 z).

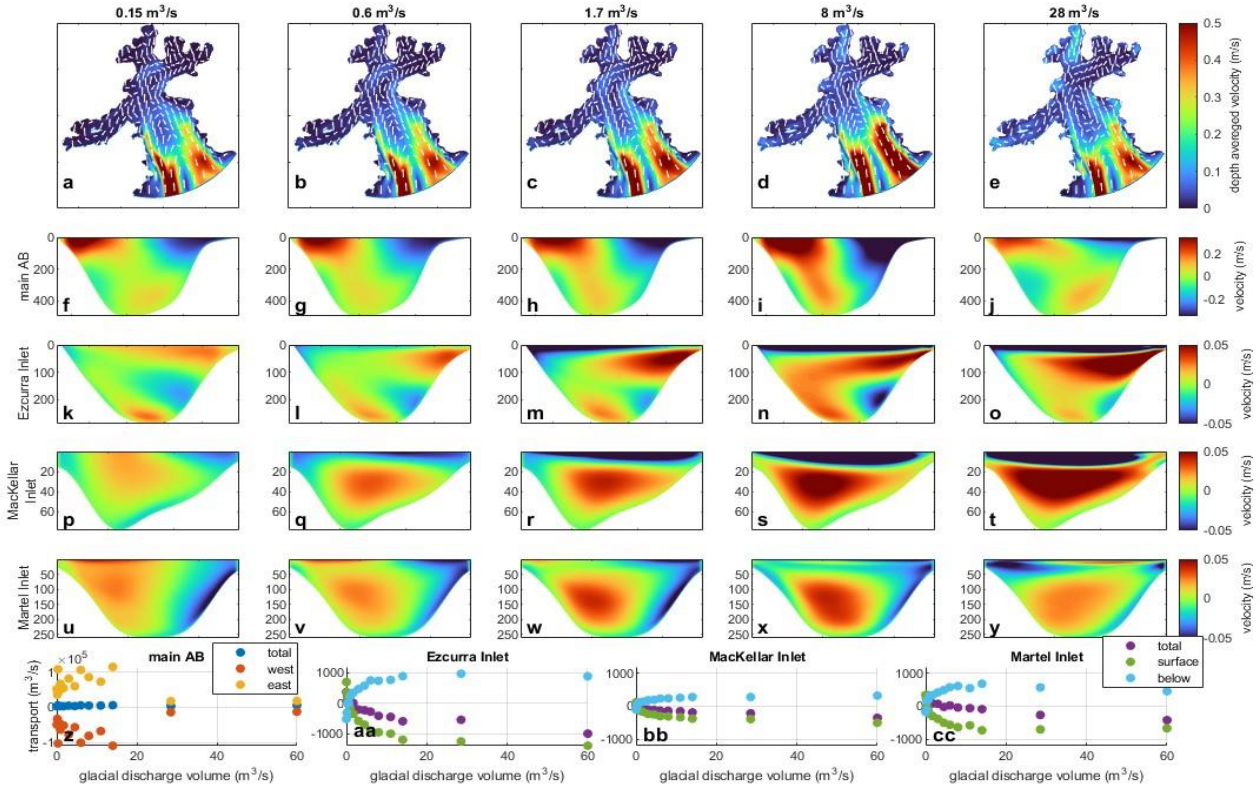

Figure 7. AB circulation influenced by growing glacial influx (five chosen model scenarios' results); **a-e.** flow depth averaged velocities in whole AB; **f-y**. velocity throughout cross-sections (locations in Fig 6 a.); **z.** variability in mean transport through cross-section main AB in total and divided into western and eastern half; **aa-cc.** variability in transport through AB inlets: total and divided into surface and below surface layers; for ff-cc. positive values =inflow, negative =outflow. All values are average for the period 1.01.2022-28.01.2022.

In order to enhance the understanding of the spatial extent of areas in which glacial bay buoyancy-driven vertical circulation can be a dominant flow pattern, maps depicting the correlation coefficients between the glacial influx and flow velocities and directions have been generated (Fig. 8). The maps are shown in three versions: for the entire water column, for depths below the pycnocline, and for surface waters inside and above the pycnocline. In regions where pycnocline was not present, the entire column of water was treated as waters below the pycnocline. Correlations have been calculated for series with at least six values. In order to reduce the influence of outliers and to increase the robustness of the results, a bootstrap resampling of data was performed (Trauth, 2010).

In three inner AB inlets, the whole of Ezcurra and MacKellar Inlets, and most of Martel Inlet, there is a strong correlation between flow velocity and glacial influx (Fig. 8a–c). Overall, based on the evidence in Figs. 7 and 8, we conclude that in these areas glacial input can create vertical circulation, driving local water exchange.

In the entire water column and in the bottom layers, the distributions of correlation coefficients of flow direction changes versus glacial influx volumes do not show any discernible pattern (Fig. 8 d-e). However, in the surface waters, a distinct areas can be recognized where, with rising glacial input, water flow turns to the right in a broad area in the middle of AB and to the left in a smaller area in the east part of the main embranchment of AB (Fig. 8 f). This shows how the

GMW surface layer deflects surface water following the general circulation pattern (Fig. 5 a), redirecting it toward the AB outlet and restricting its penetration of inner bay waters.

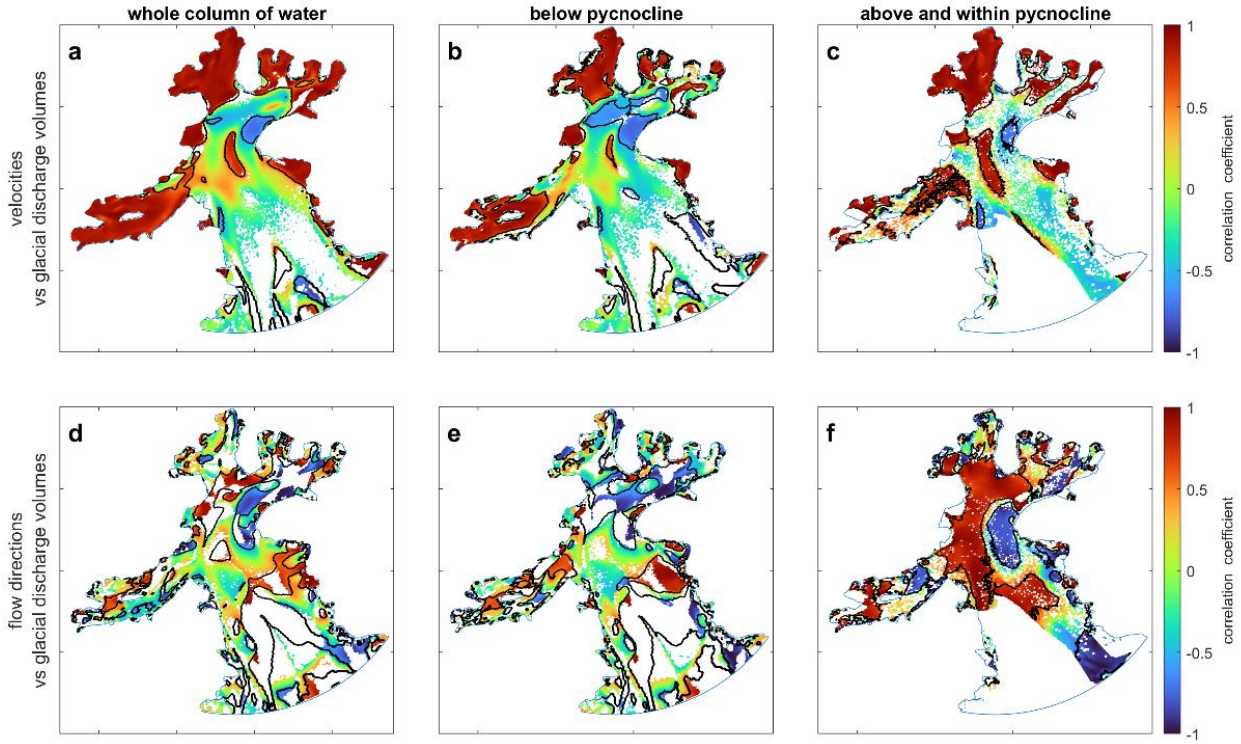

Figure 8. Correlation between rising glacial influx and flow velocities and directions; **a-c.** correlation coefficients between flow velocities and glacial discharge volumes; **d-f.** correlation coefficients between flow directions and glacial discharge volumes; positive values correspond to flow turning to the right, negative to the left; a and d. average value over the water column; **b** and **e**. below pycnocline; **c** and **f** above and within pycnocline. Areas within black boundaries contain statistically significant values.

5 Assessment of seasonal variability in glacial influx volume

Ice mass balance models, such as the Regional Atmospheric Climate Model (RACMO2, Wessem & Laffin, 2020), are commonly used to predict glacial influx volumes (Mankoff et al., 2016; Xu et al., 2012). However, due to its coarse scale in both time and space, as well as considerable uncertainty in its results (Cape et al., 2019; Mernild et al., 2010), a more locally conformable method has been developed.

Estimates of glacial input volume into AB were obtained by comparing FWT values from hydrographic observations to FWT values from 14 model scenarios, at grid points nearest to measurement site locations. A best-fitting scenario was identified for each site, per measurement day, as one with the smallest FWT difference from the FWT in measurement. The results for each day were summarized in a boxplot (Fig. 9 a), displaying a range in glacial influx volumes of best-fitting scenarios for each day across all locations.

Fig. 9 shows that the range of glacial discharge volumes employed in modeling was reasonable: the maximum glacial influx scenario of *60 m^3/s* never fits best to observed results, and the second greatest scenario of *28 m^3/s* fits best once. Fig. 9 a. depicts how winter and spring glacial influx values are close to 0 m^3/s, while continuous highest discharge volumes occur in

late summer and autumn, reaching a maximum daily median value of 8 m^3/s. The median value of projected glacial influx volume is comparatively low, maximally 0.6 m^3/s in the summer (Fig 9 b). This observation implies that periods characterized by significant glacial influx are of limited duration.

Fig. 9 c illustrates the seasonal average difference between the 75th and 25th percentiles of glacial influx estimates obtained from all sites on one measuring day. Their high values (max 2.32 m^3/s), particularly during the summer, imply that the model does not completely capture circulation in AB, most likely due to the unrealistic assumption of homogeneous and constant volumes of injections from all glaciers. This is supported by differences in median values between zones, as seen in Fig. 9 b. However, due to the long-lasting nature and high level of detail in the collected data, it is possible to generate estimates of the glacial discharge volumes to AB. During the winter and spring, the average daily median of glacial influx estimates is 0.11 and 0.09 m^3/s, respectively. It rises to 0.39 m^3/s in the autumn and peaks in the summer at 1.19 m^3/s of estimated average glacial discharge per ~1 km of glacial front.

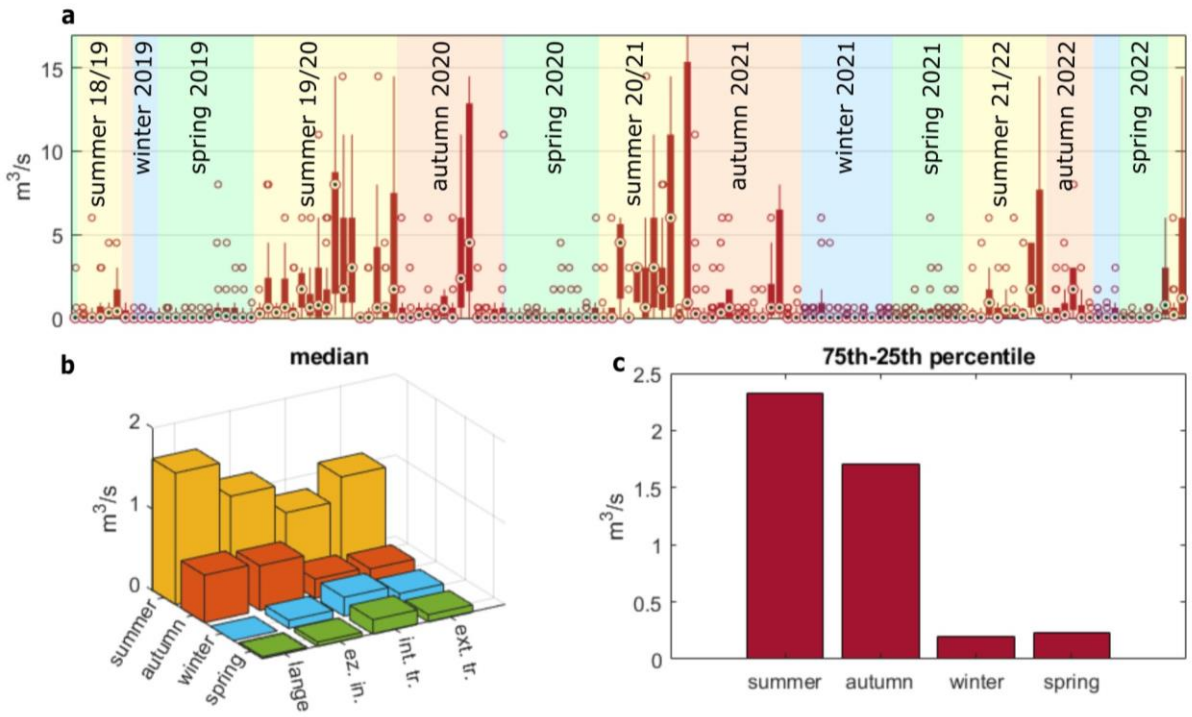

Figure 9. Estimation of glacial influx into AB assessed via a comparison of modeling and hydrographic measurement results; **a.** Glacial influx volume of scenarios with the smallest FWT difference from the measurement FWT (best-fitting scenario), in each boxplot information from all sites per measurement day (central mark=median, bottom and top edges of the box=25th and 75th percentiles, whiskers=extreme points, circles=outliers); **b.** median of glacial influx volumes from best-fitting scenarios of each day averaged per season and zone; **c.** difference between the 75th and 25th percentile of glacial influx volumes from best-fitting scenarios of each day averaged per season

6 Discussion and conclusions

The scale of the analysis is critical when examining ocean-cryosphere interactions. Straneo & Cenedese (2015) defined three glacial bay regions: the ice-ocean boundary zone, the glacial plume region, and the major fjord system. The current research focuses on AB hydrodynamics at this third scale. In this broad perspective, the vertical placement of glacial

discharges and their initial velocity has no significant impact on the overall AB circulation. This conclusion could help investigate the hydrodynamics of other similar bays in the WAP region.

A novel method of estimating glacial influx volume has been implemented and evaluated. This methodology uses a comparison of hydrographic measurements and modeling results, utilizing an exceptionally extensive dataset to affirm the validity of its findings. Other studies estimating glacial influx quantities frequently employed far fewer observational data than the 1830 measurements used in this study (Mortensen et al., 2013; Straneo & Cenedese, 2015; Sutherland et al., 2014).

The volume of glacial water released into AB is estimated to be 0.525 Gt/year (0.117 Gt/month in summer, 0.038 Gt/month in autumn, 0.011 Gt/month in winter, and 0.009 Gt/month in spring). This value is comparable to the findings of Hahn-Woernle et al. (2020), who estimated glacial influx in Andvord Bay to be 0.128 Gt/month in the summer. It is, however, significantly less than the glacial fluxes estimated for northern hemisphere fjords (De Andrés et al., 2020; Mernild et al., 2010). In Spitsbergen, the percentage share of glacial freshwater in the overall bay water budget was estimated to be around 1% (Cottier et al., 2010), in Greenlandic-based modeling, it was up to 0.25% in a medium-sized plume (Cowton et al., 2015). In the summer, on average, the glacial freshwater contribution of the AB water budget is in the range of 0.19 to 0.23% (0.9–1.7 m^3/s scenario results; see Fig. S5). Also, FWT in AB is lower than in, for example, Sermilik and Kangerdlugaauqq Greenlandic fjords, where in the summer it consistently exceeded 10 m (Sutherland et al., 2014), and in AB, even in implausible maximum high glacial influx scenarios, it seldom exceeded 3 m. This is due to relatively low glacial input volumes as well as ocean-driven circulation that carries GMW out of AB in a thin surface layer, a phenomenon observed in other Antarctic bays by Hahn-Woernle et al. (2020) and Meredith et al. (2018).

In AB the estimated glacial influx volumes rise more than ten times between spring/winter season and summer. These significant seasonal variation can be attributed to the absence of external warm water masses stimulating submarine melt during cold months, process demonstrated in studies conducted in Greenlandic fjords (Mortensen et al., 2013; Straneo et al., 2011) and in WAP region (Cape et al., 2019; Cook et al., 2016). This fluctuation may also be exacerbated by the fact that the majority of AB glaciers are shallowly grounded, causing melt to be primarily driven by external heat rather than hydrostatic pressure (Jenkins, 2011).

Hydrographic measurements and model results showed that AB water properties varied modestly throughout the year (Fig. 2 and Fig. S1), with a temperature standard deviation from all measurements of 0.90˚ C, and a salinity standard deviation of 0.22 PSU. GMW has always been the most buoyant water mass, occurring at the surface of the water column in a layer with a maximum thickness of 50–60 m, spreading in a distinctive pattern along the eastern boundary of AB, generated by the AB general circulation pattern. The temperature of glacial water exhibits slight variations compared to AW, being either colder or warmer than AW at the moment of discharge. The GMW surface layer can undergo either warming or cooling as a consequence of atmospheric forcing, dependent on the air temperature.

By integrating the findings of glacial influx estimation from Section 5 with the analysis of the impact of different volumes of glacial discharge on water level shifts and circulation from Sections 4.3.1 and 4.3.2, it can be inferred that glacial influx does not alter the general hydrodynamics of AB. The double-celled horizontal circulation pattern, which regulates water

718 exchange between AB and the ocean, has been observed to persist consistently throughout the
719 year. Unlike the findings of Mortensen et al. (2013) and Straneo et al. (2011) in Greenland, no
720 distinct modes of circulation specific to different seasons were identified in the whole AB.
721 However, in the Ezcurra, MacKellar, and inner parts of Martel inlets, the presence of GMW can
722 lead to the formation of buoyancy-driven vertical circulation. This circulation is expected to
723 occur most of the time during the summer and beginning of the autumn (estimates of glacial
724 input > 0.6 m^3/s) and to be particularly robust during short-term peak melt events (Figs. 7 and 9).

725 It is suspected that there exists a threshold volume of glacial influx, estimated to be
726 within the range of 14 to 28 m^3/s. GMW is expected to significantly limit the interchange of
727 water between the AB and the ocean above this threshold (Fig. 7 z-cc), since the ocean induced
728 general circulation in the AB is most intense at the surface, at the level in which GMW is
729 transported outside AB. The estimated amounts of glacial influx at any given point of the
730 analyzed period did not reach this level, although it is not implausible given the projected
731 increase in melt rates in this region. Hence, it is crucial to validate and investigate this process
732 further.

733 The current investigation uncovered features of Antarctic glacier bay hydrodynamics that
734 set it apart from the better-known fjords of the northern hemisphere. These differences are
735 caused by the geomorphology of the region and different relative contributions of external forces
736 acting upon bay waters. In order to accommodate these conditions, innovative approaches have
737 been utilized to investigate bay hydrodynamics, which could be useful in similar locations. These
738 entail evaluating the significance of initial velocity and vertical position of glacial influx for
739 general hydrodynamics of a bay and using a comparative study between measurements and
740 modeled data from various model scenarios to estimate glacial influx volumes.

741 This study provides a comprehensive analysis of the hydrodynamic response of an
742 Antarctic bay to changes in magnitude of glacial influx. Furthermore, with a large number of
743 data points and high temporal resolution, this study offers, to the best of our knowledge, the most
744 comprehensive assessment of seasonal variations in glacial discharge volumes to date. This
745 enables the prediction of variations in circulation within a glacial bay over the course of a year.

746 Acknowledgments

747 This work was supported by two grants from the National Science Centre, Poland: No.
748 2017/25/B/ST10/02092 ‘Quantitative assessment of sediment transport from glaciers of South
749 Shetland Islands on the basis of selected remote sensing methods’ and No.
750 2018/31/B/ST10/00195 ‘Observations and modeling of sea ice interactions with the atmospheric
751 and oceanic boundary layers’. Special thanks are owed to Laboratory of Sedimentary and
752 Environmental Processes - INCT-Criosfera Fluminense Federal University - Geoscience Institute
753 in Brazil for providing us with bathymetric data from Admiralty Bay, described in (Magrani et
754 al., 2016). We are thankful to Deltares for making Delft3D Flow model available for
755 calculations. Calculations were made possible thanks to computing power and software provided
756 by CI TASK (Center of the Tri-City Academic Computer Network) in Gdańsk, Poland. We are
757 grateful for the support of Arctowski Polish Antarctic Station’s crew for all their help during
758 measurement campaign.

Open Research

The hydrological measurement data is available at PANGAEA repository via https://doi.org/10.1594/PANGAEA.947909. The data is licensed under CC-BY-4.0. Currently, the repository contains data up until January 2022. Remaining dataset up until February 2023 is available at Zenodo repository via 10.5281/zenodo.10277429, licensed under CC-BY-4.0.

Mean values of freshwater thickness, pycnocline depth, and depth averaged velocities from modeling from 17 scenarios (14 scenarios of rising glacial influx scenarios + 3 scenarios testing importance of glacial influx vertical location and initial velocity). The mean values span the period from 1.01.2022 to 28.01.2022 and are available at Zenodo repository via 10.5281/zenodo.10277333, licensed under CC-BY-4.0.

The 65936 version of Delft3D4 model available at https://oss.deltares.nl/web/delft3d was used to calculate AB hydrodynamical model.

The bathymetric measurement data was made available to us by Laboratory of Sedimentary and Environmental Processes - INCT-Criosfera Fluminense Federal University - Geoscience Institute in Brazil.

Tide data used in modelling was derived from CATS2008 model described by Padman et al. (2002) available at https://doi.org/10.15784/601235 and is licensed under CC-BY-4.0

Reanalysis data for open boundary temperature and salinity conditions, described by Dotto et al. (2021) is available at Zenodo repository at https://doi.org/10.5281/zenodo.4420006. The data is licensed under CC-BY-4.0.

The ocean boundaries were derived from Gerrish et al. (2021) dataset available at https://doi.org/10.5285/e46be5bc-ef8e-4fd5-967b-92863fbe2835 under license CC-BY-4.0.

References

De Andrés, E., Slater, D. A., Straneo, F., Otero, J., Das, S., & Navarro, F. (2020). Surface emergence of glacial plumes determined by fjord stratification. *Cryosphere*, *14*(6), 1951–1969. https://doi.org/10.5194/TC-14-1951-2020

Bartholomaus, T. C., Larsen, C. F., & O'Neel, S. (2013). Does calving matter? Evidence for significant submarine melt. *Earth and Planetary Science Letters*, *380*, 21–30. https://doi.org/10.1016/j.epsl.2013.08.014

Battke, Z. (1990). Admiralty Bay, King George Island 1:50.000 map. *Insitute of Ecology PAS*.

Bers, A. V., Momo, F., Schloss, I. R., & Abele, D. (2013). Analysis of trends and sudden changes in long-term environmental data from King George Island (Antarctica): Relationships between global climatic oscillations and local system response. *Climatic Change*, *116*(3–4), 789–803. https://doi.org/10.1007/s10584-012-0523-4

Cape, M. R., Vernet, M., Pettit, E. C., Wellner, J., Truffer, M., Akie, G., et al. (2019). Circumpolar deep water impacts glacial meltwater export and coastal biogeochemical cycling along the west Antarctic Peninsula. *Frontiers in Marine Science*, *6*(MAR), 144. https://doi.org/10.3389/FMARS.2019.00144/BIBTEX

Carbotte, S. M., Ryan, W. B. F., Hara, S. O., Arko, R., Goodwillie, A., Melkonian, A., et al. (2007). Antarctic Multibeam Bathymetry and Geophysical Data Synthesis : An On-Line

Digital Data Resource for Marine Geoscience Research in the Southern Ocean. *10th International Symposium on Antarctic Earth Sciences*, *196*.

Carroll, D., Sutherland, D. A., Hudson, B., Moon, T., Catania, G. A., Shroyer, E. L., et al. (2016). The impact of glacier geometry on meltwater plume structure and submarine melt in Greenland fjords. *Geophysical Research Letters*, *43*(18), 9739–9748. https://doi.org/10.1002/2016GL070170

Chauché, N., Hubbard, A., Gascard, J. C., Box, J. E., Bates, R., Koppes, M., et al. (2014). Ice-ocean interaction and calving front morphology at two west Greenland tidewater outlet glaciers. *Cryosphere*, *8*(4), 1457–1468. https://doi.org/10.5194/tc-8-1457-2014

Clarke, A., Meredith, M. P., Wallace, M. I., Brandon, M. A., & Thomas, D. N. (2008). Seasonal and interannual variability in temperature, chlorophyll and macronutrients in northern Marguerite Bay, Antarctica. *Deep-Sea Research Part II: Topical Studies in Oceanography*. https://doi.org/10.1016/j.dsr2.2008.04.035

Cook, A. J., Holland, P. R., Meredith, M. P., Murray, T., Luckman, A., & Vaughan, D. G. (2016). Ocean forcing of glacier retreat in the western Antarctic Peninsula. *Science*, *353*(6296), 283–286. https://doi.org/10.1126/SCIENCE.AAE0017/SUPPL_FILE/COOK-SM.PDF

Cottier, F. R., Nilsen, F., Skogseth, R., Tverberg, V., Skarðhamar, J., & Svendsen, H. (2010). Arctic fjords: a review of the oceanographic environment and dominant physical processes. *Geological Society, London, Special Publications*, *344*(1), 35–50. https://doi.org/10.1144/SP344.4

Cottier, F. R., Nilsen, F., Skogseth, R., Tverberg, V., Skardhamar, J., & Svendsen, H. (2010). Arctic fjords: A review of the oceanographic environment and dominant physical processes. *Geological Society Special Publication*, *344*, 35–50. https://doi.org/10.1144/SP344.4

Cowton, T., Slater, D., Sole, A., Goldberg, D., & Nienow, P. (2015). Modeling the impact of glacial runoff on fjord circulation and submarine melt rate using a new subgrid-scale parameterization for glacial plumes. *Journal of Geophysical Research: Oceans*, *120*(2). https://doi.org/10.1002/2014JC010324

Deltares. (2020). Delft3D 3D/2D modelling suite for integral water solutions Hydro-Morphodynamics. *User Manual*.

Dotto, T. S., Mata, M. M., Kerr, R., & Garcia, C. A. E. (2021). A novel hydrographic gridded data set for the northern Antarctic Peninsula. *Earth System Science Data*, *13*(2), 671–696. https://doi.org/10.5194/ESSD-13-671-2021

Eayrs, C., Li, X., Raphael, M. N., & Holland, D. M. (2021). Rapid decline in Antarctic sea ice in recent years hints at future change. *Nature Geoscience*. https://doi.org/10.1038/s41561-021-00768-3

Forsch, K. O., Hahn-Woernle, L., Sherrell, R. M., Roccanova, V. J., Bu, K., Burdige, D., et al. (2021). Seasonal dispersal of fjord meltwaters as an important source of iron and manganese to coastal Antarctic phytoplankton. *Biogeosciences*, *18*(23), 6349–6375. https://doi.org/10.5194/BG-18-6349-2021

Gerrish, L., Fretwell, P., & Cooper, P. (2021). *High resolution vector polylines of the Antarctic coastline (7.4) [Data set]*. https://doi.org/https://doi.org/10.5285/e46be5bc-ef8e-4fd5-967b-92863fbe2835

Gregory, J. M., White, N. J., Church, J. A., Bierkens, M. F. P., Box, J. E., Van Den Broeke, M. R., et al. (2013). Twentieth-century global-mean sea level rise: Is the whole greater than the sum of the parts? *Journal of Climate*, *26*(13). https://doi.org/10.1175/JCLI-D-12-00319.1

Hahn-Woernle, L., Powell, B., Lundesgaard, Ø., & van Wessem, M. (2020). Sensitivity of the summer upper ocean heat content in a Western Antarctic Peninsula fjord. *Progress in Oceanography*, *183*, 102287. https://doi.org/10.1016/J.POCEAN.2020.102287

Hofmann, E. E., Klinck, J. M., Lascara, C. M., & Smith, D. A. (2011). Water mass distribution and circulation west of the Antarctic Peninsula and including Bransfield Strait. https://doi.org/10.1029/ar070p0061

Holfort, J., Hansen, E., Østerhus, S., Dye, S., Jónsson, S., Meincke, J., et al. (2008). Freshwater Fluxes East of Greenland. In *Arctic–Subarctic Ocean Fluxes* (pp. 263–287). Dordrecht: Springer Netherlands. https://doi.org/10.1007/978-1-4020-6774-7_12

IPCC. (2022). Sea Level Rise and Implications for Low-Lying Islands, Coasts and Communities. In *The Ocean and Cryosphere in a Changing Climate*. https://doi.org/10.1017/9781009157964.012

Jenkins, A. (1999). The impact of melting ice on ocean waters. *Journal of Physical Oceanography*. https://doi.org/10.1175/1520-0485(1999)029<2370:TIOMIO>2.0.CO;2

Jenkins, A. (2011). Convection-Driven Melting near the Grounding Lines of Ice Shelves and Tidewater Glaciers. *Journal of Physical Oceanography*, *41*(12), 2279–2294. https://doi.org/10.1175/JPO-D-11-03.1

Jenkins, A., & Jacobs, S. (2008). Circulation and melting beneath George VI Ice Shelf, Antarctica. *Journal of Geophysical Research*, *113*(C4), C04013. https://doi.org/10.1029/2007JC004449

Lundesgaard, Ø., Powell, B., Merrifield, M., Hahn-Woernle, L., & Winsor, P. (2019). Response of an Antarctic Peninsula Fjord to Summer Katabatic Wind Events. *Journal of Physical Oceanography*, *49*(6), 1485–1502. https://doi.org/10.1175/JPO-D-18-0119.1

Lundesgaard, Ø., Winsor, P., Truffer, M., Merrifield, M., Powell, B., Statscewich, H., et al. (2020). Hydrography and energetics of a cold subpolar fjord: Andvord Bay, western Antarctic Peninsula. *Progress in Oceanography*, *181*, 102224. https://doi.org/10.1016/j.pocean.2019.102224

Magrani, F., Neto, A. A., & Vieira, R. (2016). Glaciomarine sedimentation and submarine geomorphology in Admiralty Bay, South Shetland Islands, Antarctica. *2015 IEEE/OES Acoustics in Underwater Geosciences Symposium, RIO Acoustics 2015*. https://doi.org/10.1109/RIOACOUSTICS.2015.7473614

Majdański, M., Środa, P., Malinowski, M., Czuba, W., Grad, M., Guterch, A., & Hegedűs, E. (2008). 3D seismic model of the uppermost crust of the Admiralty Bay area, King George Island, West Antarctica. *Polar Res*, *29*(4), 303–318.

879 Mankoff, K. D., Straneo, F., Cenedese, C., Das, S. B., Richards, C. G., & Singh, H. (2016).
880 Structure and dynamics of a subglacial discharge plume in a Greenlandic fjord. *Journal of*
881 *Geophysical Research: Oceans*. https://doi.org/10.1002/2016JC011764

882 Meredith, M. P., & King, J. C. (2005). Rapid climate change in the ocean west of the Antarctic
883 Peninsula during the second half of the 20th century. *Geophysical Research Letters*, *32*(19),
884 n/a-n/a. https://doi.org/10.1029/2005GL024042

885 Meredith, M. P., Wallace, M. I., Stammerjohn, S. E., Renfrew, I. A., Clarke, A., Venables, H. J.,
886 et al. (2010). Changes in the freshwater composition of the upper ocean west of the
887 Antarctic Peninsula during the first decade of the 21st century. *Progress in Oceanography*,
888 *87*(1–4), 127–143. https://doi.org/10.1016/J.POCEAN.2010.09.019

889 Meredith, M. P., Falk, U., Bers, A. V., Mackensen, A., Schloss, I. R., Barlett, E. R., et al. (2018).
890 Anatomy of a glacial meltwater discharge event in an Antarctic cove. *Philosophical*
891 *Transactions of the Royal Society A: Mathematical, Physical and Engineering Sciences*,
892 *376*(2122). https://doi.org/10.1098/rsta.2017.0163

893 Mernild, S. H., Howat, I. M., Ahn, Y., Liston, G. E., Steffen, K., Jakobsen, B. H., et al. (2010).
894 Freshwater flux to Sermilik Fjord, SE Greenland. *Cryosphere*, *4*(4).
895 https://doi.org/10.5194/tc-4-453-2010

896 Moffat, C., & Meredith, M. (2018). Shelf–ocean exchange and hydrography west of the
897 Antarctic Peninsula: a review. *Philosophical Transactions of the Royal Society A:*
898 *Mathematical, Physical and Engineering Sciences*, *376*(2122), 20170164.
899 https://doi.org/10.1098/rsta.2017.0164

900 Moffat, C., Owens, B., & Beardsley, R. C. (2009). On the characteristics of Circumpolar Deep
901 Water intrusions to the west Antarctic Peninsula Continental Shelf. *Journal of Geophysical*
902 *Research: Oceans*, *114*(5). https://doi.org/10.1029/2008JC004955

903 Monien, D., Monien, P., Brünjes, R., Widmer, T., Kappenberg, A., Silva Busso, A. A., et al.
904 (2017). Meltwater as a source of potentially bioavailable iron to Antarctica waters.
905 *Antarctic Science*, *29*(3), 277–291. https://doi.org/10.1017/S095410201600064X

906 Mortensen, J., Bendtsen, J., Motyka, R. J., Lennert, K., Truffer, M., Fahnestock, M., &
907 Rysgaard, S. (2013). On the seasonal freshwater stratification in the proximity of fast-
908 flowing tidewater outlet glaciers in a sub-Arctic sill fjord. *Journal of Geophysical*
909 *Research: Oceans*, *118*(3), 1382–1395. https://doi.org/10.1002/jgrc.20134

910 Motyka, R. J., Hunter, L., Echelmeyer, K. A., & Connor, C. (2003). Submarine melting at the
911 terminus of a temperate tidewater glacier, LeConte Glacier, Alaska, U.S.A. *Annals of*
912 *Glaciology*. https://doi.org/10.3189/172756403781816374

913 National Snow and Ice Data Center, C. (2023). Sea Ice Index. Retrieved June 7, 2023, from
914 https://nsidc.org/data/seaice_index

915 Naughten, K. A., Holland, P. R., & De Rydt, J. (2023). Unavoidable future increase in West
916 Antarctic ice-shelf melting over the twenty-first century. *Nature Climate Change*.
917 https://doi.org/10.1038/s41558-023-01818-x

918 Osińska, M., Bialik, R. J., & Wójcik-Długoborska, K. A. (2021). Interrelation of quality
919 parameters of surface waters in five tidewater glacier coves of King George Island,

Antarctica. *Science of the Total Environment*, *771*, 144780. https://doi.org/10.1016/j.scitotenv.2020.144780

Osińska, M., Wójcik-Długoborska, K. A., & Bialik, R. J. (2022). Water conductivity, salinity, temperature, turbidity, pH, fluorescent dissolved organic matter (fDOM), optical dissolved oxygen (ODO), chlorophyll a and phycoerythrin measurements in Admiralty Bay, King George Island, from Dec 2018 to Jan 2022. *PANGAEA*. https://doi.org/https://doi.org/10.1594/PANGAEA.947909

Osińska, M., Wójcik-Długoborska, K. A., & Bialik, R. J. (2023). Annual hydrographic variability in Antarctic coastal waters infused with glacial inflow. *Earth System Science Data*, *15*(2). https://doi.org/10.5194/essd-15-607-2023

Padman, L., Fricker, H. A., Coleman, R., Howard, S., & Erofeeva, L. (2002). A new tide model for the Antarctic ice shelves and seas. https://doi.org/10.3189/172756402781817752

Plenzler, J., Budzik, T., Puczko, D., & Bialik, R. J. (2019). Climatic conditions at Arctowski Station (King George Island, West Antarctica) in 2013-2017 against the background of regional changes. *Polish Polar Research*, *40*(1), 1–27. https://doi.org/10.24425/PPR.2019.126345

Potapowicz, J., Szumińska, D., Szopińska, M., Bialik, R. J., Machowiak, K., Chmiel, S., & Polkowska, Ż. (2020). Seashore sediment and water chemistry at the Admiralty Bay (King George Island, Maritime Antarctica) – Geochemical analysis and correlations between the concentrations of chemical species. *Marine Pollution Bulletin*, *152*, 110888. https://doi.org/10.1016/J.MARPOLBUL.2020.110888

Poulin, F. J., Stegner, A., Hernández-Arencibia, M., Marrero-Díaz, A., & Sangrà, P. (2014). Steep shelf stabilization of the coastal bransfield current: Linear stability analysis. *Journal of Physical Oceanography*. https://doi.org/10.1175/JPO-D-13-0158.1

Powell, R., & Domack, G. W. (2002). Modern glaciomarine environments. *Modern and Past Glacial Environments*, 361–389. https://doi.org/10.1016/B978-075064226-2/50015-5

Robakiewicz, M., & Rakusa-Suszczewski, S. (1999). Application of 3D circulation model to Admiralty Bay, King George Island, Antarctica. *Polish Polar Research*, *20*(1), 43–58.

Rückamp, M., Blindow, N., Suckro, S., Braun, M., & Humbert, A. (2010). Dynamics of the ice cap on King George Island, antarctica: Field measurements and numerical simulations. *Annals of Glaciology*, *51*(55), 80–90. https://doi.org/10.3189/172756410791392817

Sangrà, P., Gordo, C., Hernández-Arencibia, M., Marrero-Díaz, A., Rodríguez-Santana, A., Stegner, A., et al. (2011). The Bransfield current system. *Deep-Sea Research Part I: Oceanographic Research Papers*. https://doi.org/10.1016/j.dsr.2011.01.011

Schloss, I. R., Abele, D., Moreau, S., Demers, S., Bers, A. V., González, O., & Ferreyra, G. A. (2012). Response of phytoplankton dynamics to 19-year (1991–2009) climate trends in Potter Cove (Antarctica). *Journal of Marine Systems*, *92*(1), 53–66. https://doi.org/10.1016/j.jmarsys.2011.10.006

Sciascia, R., Straneo, F., Cenedese, C., & Heimbach, P. (2013). Seasonal variability of submarine melt rate and circulation in an East Greenland fjord. *Journal of Geophysical Research: Oceans*, *118*(5), 2492–2506. https://doi.org/10.1002/jgrc.20142

961 Simões, J. C., Bremer, U. F., Aquino, F. E., & Ferron, F. A. (1999). Morphology and variations
962 of glacial drainage basins in the King George Island ice field, Antarctica. *Annals of*
963 *Glaciology*, *29*, 220–224. https://doi.org/10.3189/172756499781821085

964 Slater, D. A., Straneo, F., Das, S. B., Richards, C. G., Wagner, T. J. W., & Nienow, P. W.
965 (2018). Localized Plumes Drive Front-Wide Ocean Melting of A Greenlandic Tidewater
966 Glacier. *Geophysical Research Letters*, *45*(22), 12,350-12,358.
967 https://doi.org/10.1029/2018GL080763

968 Spall, M. A., Jackson, R. H., & Straneo, F. (2017). Katabatic Wind-Driven Exchange in Fjords.
969 *Journal of Geophysical Research: Oceans*, *122*(10), 8246–8262.
970 https://doi.org/10.1002/2017JC013026

971 Straneo, Fiamma, & Cenedese, C. (2015). The Dynamics of Greenland's Glacial Fjords and
972 Their Role in Climate. *Annual Review of Marine Science*, *7*(1), 89–112.
973 https://doi.org/10.1146/annurev-marine-010213-135133

974 Straneo, Fiammetta, Curry, R., Sutherland, D., Hamilton, G., Cenedese, C., Vaage, K., &
975 Stearns, L. (2011). Impact of ocean stratification on submarine melting of a major
976 Greenland outlet glacier. *Nature Precedings*. https://doi.org/10.1038/npre.2011.5670.1

977 Sutherland, D. A., Straneo, F., & Pickart, R. S. (2014). Characteristics and dynamics of two
978 major Greenland glacial fjords. *Journal of Geophysical Research: Oceans*, *119*(6), 3767–
979 3791. https://doi.org/10.1002/2013JC009786

980 Thompson, A. F., Heywood, K. J., Thorpe, S. E., Renner, A. H. H., & Trasviña, A. (2009).
981 Surface Circulation at the Tip of the Antarctic Peninsula from Drifters. *Journal of Physical*
982 *Oceanography*, *39*(1), 3–26. https://doi.org/10.1175/2008JPO3995.1

983 Trauth, M. H. (2010). *MATLAB® recipes for earth sciences: Third edition*. *MATLAB® Recipes*
984 *for Earth Sciences (Third Edition)*. https://doi.org/10.1007/978-3-642-12762-5

985 Valle-Levinson, A. (2010). Contemporary Issues in Estuarine Physics. *Contemporary Issues in*
986 *Estuarine Physics*, 1–315. https://doi.org/10.1017/CBO9780511676567

987 Valle-Levinson, A. (Arnoldo). (2022). *Introduction to estuarine hydrodynamics*. Cambridge
988 University Press. Retrieved from
989 https://books.google.com/books/about/Introduction_to_Estuarine_Hydrodynamics.html?hl=
990 pl&id=2PKazgEACAAJ

991 Vaughan, D. G. (2006). Recent trends in melting conditions on the Antarctic Peninsula and their
992 implications for ice-sheet mass balance and sea level. *Arctic, Antarctic, and Alpine*
993 *Research*, *38*(1). https://doi.org/10.1657/1523-0430(2006)038[0147:RTIMCO]2.0.CO;2

994 Wessem, J. M. V., & Laffin, M. K. (2020). Regional Atmospheric Climate Model 2 (RACMO2),
995 version 2.3p2 (2.3p2) [Data set].

996 Xu, Y., Rignot, E., Menemenlis, D., & Koppes, M. (2012). Numerical experiments on
997 subaqueous melting of Greenland tidewater glaciers in response to ocean warming and
998 enhanced subglacial discharge. *Annals of Glaciology*, *53*(60), 229–234.
999 https://doi.org/10.3189/2012AoG60A139

1000 Zhou, M., Niiler, P. P., & Hu, J. H. (2002). Surface currents in the Bransfield and Gerlache
1001 Straits, Antarctica. *Deep Sea Research Part I: Oceanographic Research Papers*, *49*(2),
1002 267–280. https://doi.org/10.1016/S0967-0637(01)00062-0

1003 Zhou, M., Niiler, P. P., Zhu, Y., & Dorland, R. D. (2006). The western boundary current in the
1004 Bransfield Strait, Antarctica. *Deep-Sea Research Part I: Oceanographic Research Papers*.
1005 https://doi.org/10.1016/j.dsr.2006.04.003

1006 Zhou, X., Zhu, G., & Hu, S. (2020). Influence of tides on mass transport in the Bransfield Strait
1007 and the adjacent areas, Antarctic. *Polar Science*, *23*, 100506.
1008 https://doi.org/10.1016/J.POLAR.2020.100506

1009